This article is a *Plant Cell* Advance Online Publication. The date of its first appearance online is the official date of publication. The article has been edited and the authors have corrected proofs, but minor changes could be made before the final version is published. Posting this version online reduces the time to publication by several weeks.

LARGE-SCALE BIOLOGY ARTICLE

Comprehensive Annotation of *Physcomitrella patens* Small RNA Loci Reveals That the Heterochromatic Short Interfering RNA Pathway Is Largely Conserved in Land Plants[OPEN]

Ceyda Coruh,[a,b,c,1] Sung Hyun Cho,[c,1,2] Saima Shahid,[a,b,c] Qikun Liu,[a,b,c,3] Andrzej Wierzbicki,[d] and Michael J. Axtell[a,b,c,4]

[a] Plant Biology PhD Program, Penn State University, University Park, Pennsylvania 16802
[b] Huck Institutes of the Life Sciences, Penn State University, University Park, Pennsylvania 16802
[c] Department of Biology, Penn State University, University Park, Pennsylvania 16802
[d] Department of Molecular, Cellular, and Developmental Biology, University of Michigan, Ann Arbor, Michigan 48109

ORCID IDs: 0000-0002-8191-7181 (S.H.C.); 0000-0003-2489-2907 (Q.L.)

Many plant small RNAs are sequence-specific negative regulators of target mRNAs and/or chromatin. In angiosperms, the two most abundant endogenous small RNA populations are usually 21-nucleotide microRNAs (miRNAs) and 24-nucleotide heterochromatic short interfering RNAs (siRNAs). Heterochromatic siRNAs are derived from repetitive regions and reinforce DNA methylation at targeted loci. The existence and extent of heterochromatic siRNAs in other land plant lineages has been unclear. Using small RNA-sequencing (RNA-seq) of the moss *Physcomitrella patens*, we identified 1090 loci that produce mostly 23- to 24-nucleotide siRNAs. These loci are mostly in intergenic regions with dense DNA methylation. Accumulation of siRNAs from these loci depends upon *P. patens* homologs of *DICER-LIKE3* (*DCL3*), *RNA-DEPENDENT RNA POLYMERASE2*, and the largest subunit of *DNA-DEPENDENT RNA POLYMERASE IV*, with the largest subunit of a Pol V homolog contributing to expression at a smaller subset of the loci. A *MINIMAL DICER-LIKE* (*mDCL*) gene, which lacks the N-terminal helicase domain typical of DCL proteins, is specifically required for 23-nucleotide siRNA accumulation. We conclude that heterochromatic siRNAs, and their biogenesis pathways, are largely identical between angiosperms and *P. patens*, with the notable exception of the *P. patens*-specific use of *mDCL* to produce 23-nucleotide siRNAs.

INTRODUCTION

Small noncoding RNAs regulate gene expression to modulate growth, development, differentiation, genome silencing, and stress responses in eukaryotic organisms (Matzke and Mosher, 2014). There are two main categories of endogenous small RNAs in plants: microRNAs (miRNAs) and short interfering RNAs (siRNAs). Although the silencing pathways utilizing small RNAs have much in common, there are some fundamental distinctions between the two classes of small RNAs, particularly in regard to their biogenesis, evolutionary conservation, targets, and modes of action (Axtell, 2013a). Most importantly, miRNAs and siRNAs differ in their precursors: While siRNA precursors are the products of RNA-dependent RNA polymerase synthesized double-stranded RNA duplexes, miRNAs are derived from single RNA molecules that fold back to form self-complementary hairpin RNAs. Endogenous siRNAs are the dominant small RNA type in many plant species, while miRNAs have received more attention, particularly in regard to annotations of specific loci (Coruh et al., 2014).

Heterochromatin, which contains repetitive sequences and transposable elements, is silenced by conserved epigenetic modifications of histones and DNA. Epigenetic silencing is believed to prevent abnormal chromosomal rearrangements and activation of transposons, which can cause mutations if they are integrated into genes (Lippman and Martienssen, 2004). In flowering plants, siRNAs are known to induce DNA methylation at targeted genomic regions (Matzke and Mosher, 2014). Repressive histone modifications and siRNA-directed DNA methylation form a positive feedback loop to reinforce transcriptional silencing. This pathway is particularly well understood in *Arabidopsis thaliana*, where the presence of H3K9 methylation leads the SAWADEE HOMEODOMAIN HOMOLOG1/DNA BINDING TRANSCRIPTION FACTOR1 protein to recruit an alternative DNA-dependent RNA polymerase (Pol IV) to chromatin (Law et al., 2013; H. Zhang et al., 2013). Pol IV transcribes precursors of heterochromatic siRNAs, which are promptly converted into double-stranded RNAs by RNA-DEPENDENT RNA POLYMERASE2 (RDR2), and then processed by DICER-LIKE3

[1] These authors contributed equally to this work.
[2] Current address: Department of Biochemistry and Molecular Biology, Penn State University, University Park, PA 16802.
[3] Current address: Department of Molecular, Cell, and Developmental Biology, University of California, Los Angeles, CA 90095.
[4] Address correspondence to mja18@psu.edu.
The author responsible for distribution of materials integral to the findings presented in this article in accordance with the policy described in the Instructions for Authors (www.plantcell.org) is: Michael J. Axtell (mja18@psu.edu).
[OPEN] Articles can be viewed online without a subscription.
www.plantcell.org/cgi/doi/10.1105/tpc.15.00228

(DCL3) to generate 24-nucleotide siRNAs (Xie et al., 2004; Daxinger et al., 2009). The 24-nucleotide siRNAs are then bound to ARGONAUTE4 (AGO4) or a related AGO protein and seek nascent transcripts produced by another alternative DNA-dependent RNA polymerase, Pol V (Wierzbicki et al., 2008, 2009). Binding of an AGO4-siRNA complex to Pol V nascent transcripts is thought to recruit DNA and histone methyltransferases to the vicinity of the target chromatin.

The 24-nucleotide heterochromatic siRNAs dominate endogenous small RNA populations in most tissues of most angiosperms, but their presence in other land plants has been less clear. All of the early small RNA-sequencing (RNA-seq) efforts from the mosses *Physcomitrella patens* (Arazi et al., 2005) and *Polytrichum juniperinum* (Axtell and Bartel, 2005), several gymnosperm species (Dolgosheina et al., 2008), and the lycophyte *Selaginella moellendorffii* (Banks et al., 2011) found a conspicuous absence of endogenous 24-nucleotide RNAs. It has also been suggested that conifers lack homologs of *DCL3* (Dolgosheina et al., 2008). However, there are several hints suggesting that the heterochromatic siRNA pathway may indeed be present outside of angiosperms. Significant amounts of 24-nucleotide RNAs have been observed in conifers in a highly tissue-specific manner (Nystedt et al., 2013; J. Zhang et al., 2013). Nonconiferous gymnosperms (*Cycas* and *Gingko*) contain clear 24-nucleotide RNA populations, as does the fern *Marsilea quadrifolia* (Chávez Montes et al., 2014). The *Selaginella* genome contains *DCL3*, *RDR2*, *AGO4*, and Pol IV/V largest subunit homologs (Banks et al., 2011), suggesting that the absence of 24-nucleotide RNAs in initial small RNA-seq libraries may be due to tissue-restricted expression. Phylogenetic analysis clearly identifies *DCL3*, *AGO4*, and *Pol V*-related homologs in basal plants (Huang et al., 2015). Finally, our previous analysis demonstrated that the *P. patens DCL3* homolog is required for the accumulation of 22-, 23-, and 24-nucleotide RNAs from a handful of siRNA hot spots (Cho et al., 2008). Nonetheless, direct experimental proof of a bona fide heterochromatic siRNA system in plants basal to the angiosperms is currently lacking. In this study, we used extensive small RNA-seq analysis in wild-type and several *P. patens* mutants (two *RDR*s, Pol IV, Pol V, two canonical *DCL*s, and a minimal *DCL* gene) to rigorously test the hypothesis that heterochromatic siRNAs are expressed in this basal land plant.

RESULTS

Most *DCL*-Derived Small RNA Loci Produce Mixtures of 23- to 24-Nucleotide Small RNAs in *P. patens*

Several previous studies have annotated *P. patens* miRNAs and endogenous siRNAs using small RNA-seq (Arazi et al., 2005; Axtell et al., 2006; Fattash et al., 2007; Cho et al., 2008; Arif et al., 2012). However, these previous small RNA-seq efforts all had low sequencing depth by current standards (<0.5 million mapped reads per library in all cases). Reliability of annotating and quantifying small RNA producing loci is largely dependent on the sequencing depth. Therefore, to create a more comprehensive annotation of *P. patens* small RNA genes, we obtained 10 small RNA-seq libraries (from six biological replicates; four samples were run twice) from 10-d-old wild-type protonemata totaling more than 100 million mapped reads (Supplemental Table 1). The majority of the small RNAs aligned to the nuclear genome, while a substantial minority aligned to the plastid genome. In order to identify a reference set of small RNA genes, we first de novo annotated potential small RNA clusters separately from six wild-type small RNA libraries using ShortStack (Axtell, 2013b). Then, genomic regions that were covered by cluster annotations in at least four of the six wild-type replicates were used as our reference set of *P. patens* small RNA genes. This stringent strategy allowed us to identify 1462 small RNA-producing loci (Supplemental Data Set 1). For each locus, the fraction of included reads 20 to 24 nucleotides in length was calculated, and a cutoff of 0.8 was used to discriminate non-*DCL*-derived loci from *DCL*-derived loci. Non-*DCL*-derived small RNAs are most often breakdown products of abundant long RNAs, such as rRNA, tRNA, and mRNAs. Only 17 loci were found to have a predominant RNA size (which we refer to as the "DicerCall") outside of the *DCL* size range. Therefore, we focused on the 1445 *DCL* loci for the remainder of the study (Supplemental Data Set 1). These annotations, and all underlying data, can be interactively explored via a genome browser and other tools at http://plantsmallrnagenes.psu.edu/physcomitrella_patens/.

All annotated small RNA loci were classified into two categories: *MIRNA* loci and siRNA loci. Most *DCL*-derived small RNA loci were classified as siRNA loci (Figure 1). The majority were siRNA loci with DicerCalls of 23 or 24 (Figure 1A). However, when analyzed by total abundance, 21-nucleotide RNAs dominated both *MIRNA* and siRNA loci (Figure 1B). Thus, we conclude that a relatively small number of *MIRNA* and siRNA loci produce large amounts of 21-nucleotide RNAs, while a much larger number of mostly siRNA loci produce more modest amounts of 23- and 24-nucleotide RNAs.

DicerCall is a somewhat crude indicator and could mask cases where loci actually tend to produce mixtures of different sized RNAs. For *MIRNA* and 20- to 22-nucleotide siRNA loci, the DicerCall generally reflected a strong majority of RNAs of that size (Figures 1C and 1D). However, siRNA loci with DicerCalls of 23 or 24 in fact often produce mixtures of 23 and 24 nucleotide RNAs (Figure 1E). For further analyses, we classified three different groupings of *DCL* loci, listed here in order from most to least numerous: 23- to 24-nucleotide siRNA loci, 20- to 22-nucleotide siRNA loci, and *MIRNA* loci (Figures 1C to 1E).

P. patens 23- to 24-Nucleotide siRNA Loci Are Associated with Intergenic Regions, Repeats, and Regions with Dense 5-Methyl Cytosine

We performed co-occupancy analysis of the three groupings of *DCL*-derived small RNA loci against various genomic features. Two broad patterns were apparent. At one extreme, *MIRNA*s, and to a lesser extent 20- to 22-nucleotide siRNA loci, avoid regions with dense 5-methyl cytosine (5-mC) and repeats, but instead have some tendencies to overlap with genes (Figure 2). At the other extreme, 23- to 24-nucleotide siRNA loci are enriched for overlaps with 5-mC-dense regions of all contexts, intergenic regions, and repeats, but are severely depleted in

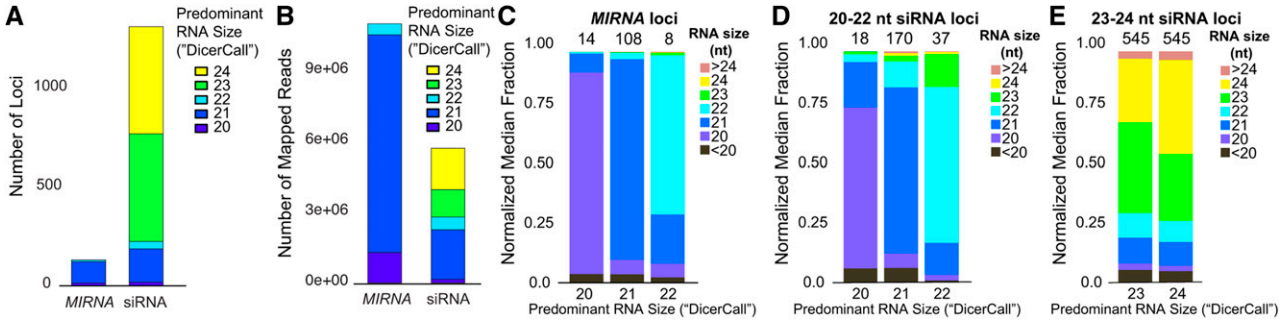

Figure 1. Properties of *P. patens* Small RNA Genes.

(A) and **(B)** Classification of *DCL*-derived small RNA loci, counted either by number of loci **(A)** or by total small RNA abundance **(B)**.
(C) to **(E)** Small RNA size distributions within each class of DicerCall at *MIRNA* loci **(C)**, 20- to 22-nucleotide siRNA loci **(D)**, and 23- to 24-nucleotide siRNA loci **(E)**.

overlaps with genes (Figures 2A and 2C). Consistent with a previous analysis (Zemach et al., 2010), *P. patens* loci with dense 5-mC are almost entirely confined to intergenic regions, enriched for association with repeats, and avoid genes (Figures 2B and 2D). It has been previously shown that Arabidopsis AGO4 preferentially binds to 24-nucleotide siRNAs with a 5′-bias toward A residues (Mi et al., 2008). Nucleotide frequency analysis revealed that small RNAs produced from 23- to 24-nucleotide siRNA loci in *P. patens* exhibit a weak 5′-A preference (Supplemental Figure 1). We conclude that *P. patens* 23- to 24-nucleotide siRNA loci are heterochromatic siRNAs, with grossly similar genomic arrangements as the heterochromatic siRNAs of angiosperms.

Improved *P. patens MIRNA* Annotations

Our entirely de novo annotation of *MIRNA*s found 130 loci, of which 112 were already annotated in miRBase release 21 (Kozomara and Griffiths-Jones, 2014) (Figure 3; Supplemental Data Sets 2 and 3). We compared our mature miRNAs from novel loci with all mature miRNAs present in miRBase release 21. Three of the novel loci were found to be paralogs of known families (miR1027c, miR1049b, and miR1034b), and the remaining 15 new loci are not easily placed in previously known plant miRNA families (Figure 3A). We also found that most abundant miRNA reads have a 5′-U bias at *P. patens MIRNA* loci (Supplemental Figure 1), similar to what is observed for AGO1-bound miRNAs in Arabidopsis (Mi et al., 2008).

miRBase release 21 lists 229 *P. patens MIRNA* loci. We were unable to align three of these hairpins to the reference genome, leaving 226 loci to consider. Among these 226 loci, 96 are annotated in miRBase 21 as “high confidence” based on older and smaller RNA-seq data sets. Our deeper data set coupled with improved *MIRNA* annotation methods allowed us to further assess these prior annotations. Most *P. patens* miRBase loci (149 out of 226) were discovered as small RNA producing loci in our analysis (Supplemental Data Set 4). Only 114 of the prior miRBase annotations satisfied the strict structure and expression criteria we imposed (Figure 3B). Interestingly, the overlap between those 114 and the loci noted as “high confidence” loci in miRBase 21 (Kozomara and Griffiths-Jones, 2014) was not very high. Only 53 of the 96 miRBase 21 high confidence loci were accepted by our analysis (Figure 3B; Supplemental Data Set 4). We attribute this to the much greater sequencing depth, and consequent increased specificity, that our new small RNA-seq data allowed.

No Evidence for Widespread 5-mC or Secondary siRNA Accumulation from *P. patens* miRNA Targets

It has been proposed that high ratios of miRNA-to-target abundance promote 5-mC modification of target gene DNA in *P. patens* (Khraiwesh et al., 2010). However, bisulfite-seq data from Zemach et al. (2010) indicated that *P. patens* genes from a wild-type specimen are largely devoid of 5-mC in all sequence contexts in genes (Figures 3C and 3D). This lack of gene body 5-mC was even more strongly apparent in a set of 42 validated miRNA targets (Addo-Quaye et al., 2009) (Figures 3C and 3D; Supplemental Data Set 5). We conclude that either the earlier hypothesis is incorrect or that none of the natural miRNA-to-target ratios in wild-type 10-d-old protonemata are high enough to promote this effect. It is also possible that miRNA-directed target DNA methylation is only seen under certain conditions, such as at a miR1026 target after abscisic acid-induced expression (Khraiwesh et al., 2010).

It has been reported that protein-coding *P. patens* miRNA targets often spawn large amounts of ~21-nucleotide secondary siRNAs both upstream and downstream of miRNA target sites (Khraiwesh et al., 2010). Despite the fact that about half of the 21- to 22-nucleotide siRNA loci we found overlapped a gene annotation (Figure 2A), only one overlapped with a validated miRNA target. This was the Pp *TAS3a* locus, a well known and deeply conserved producer of secondary siRNAs (Axtell et al., 2006) (Supplemental Data Set 5). RNA gel blots against two mRNAs that have validated as targets of conserved, highly abundant miRNAs (miR156 and miR166) failed to detect any secondary small RNA accumulation (Figures 3E and 3F). Our genome-wide analysis thus did not find evidence that *P. patens* miRNA targets generally spawn secondary siRNAs under our growth conditions.

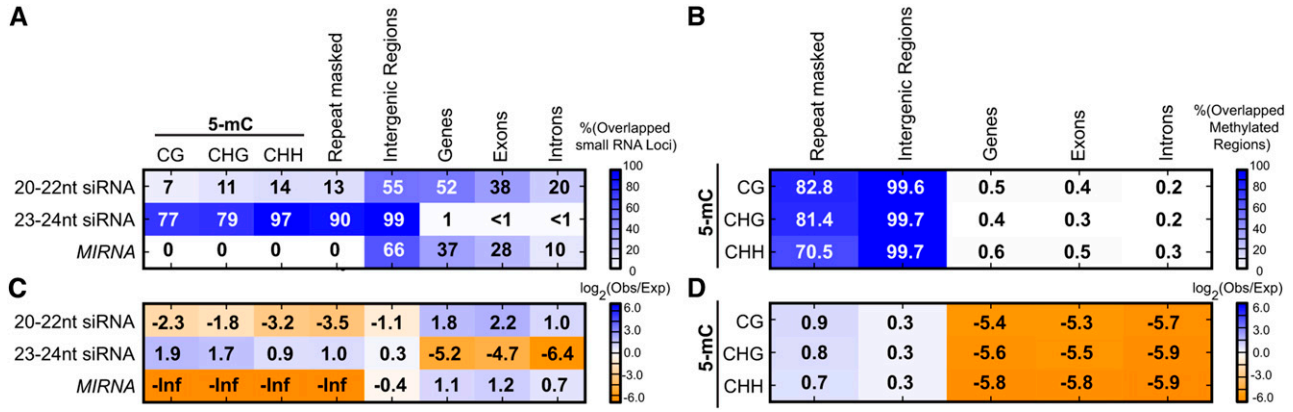

Figure 2. Genomic Features of *P. patens* Small RNA-Producing Loci.

(A) Percentages of small RNA-producing loci that overlap various genomic features: % overlap = (# small RNA loci overlapping with one or more of the indicated genomic feature/# total small RNA loci) * 100.
(B) Percentages of regions of dense DNA methylation (5-mC) in three different contexts (CG, CHG, and CHH) relative to different genomic features.
(C) Heat map showing $\log_2$ (observed overlapped bases/expected overlapped bases) for each of the pairwise comparisons shown. Small RNA loci versus various genomic features are indicated. Cell values are shown in bold text.
(D) Heat map showing $\log_2$ (observed overlapped bases/expected overlapped bases) for each of the pairwise comparisons shown. Regions of dense DNA methylation (5-mC) in three different contexts (CG, CHG, and CHH) versus various genomic features are indicated. Repeat masked: repeats of various types as annotated by the Joint Genome Initiative genome annotation.

Discovery and Mutagenesis of a *P. patens MINIMAL DICER-LIKE* Gene

Next, we revisited annotation of the *P. patens DCL* gene family. Dicers emerged early in the eukaryotic lineage and independently diverged in plants and animals (Mukherjee et al., 2013). Plants contain four ancient clades of *DCL* genes, with members in each clade being sub-functionalized for different types of small RNAs (Margis et al., 2006; Huang et al., 2015). *P. patens* has been reported to have no members of the *DCL2* clade, single members of both the *DCL3* and *DCL4* clades, and two members of the *DCL1* clade (Pp *DCL1a* and Pp *DCL1b*) (Axtell et al., 2007). Mutants in all four genes have been described (Cho et al., 2008; Khraiwesh et al., 2010; Arif et al., 2012). Upon review of *P. patens DCL* genes, we noticed several discrepancies in the annotation of the Pp *DCL1b* locus. All of the three available mRNA models were strongly contradicted by RNA-seq data (Chen et al., 2012), and none were capable of producing a full-length DCL protein (Supplemental Figure 2). *De novo* mRNA assembly using RNA-seq data resulted in several transcript models, none of which possessed any open reading frames > 100 codons in length (Supplemental Figure 2; Supplemental Data Set 6). Given these ambiguities, we excluded DCL1b when constructing a phylogeny of DCL proteins. We suspect that *DCL1b* is an expressed, spliced pseudogene.

We also identified a *P. patens MINIMAL DICER-LIKE* (*mDCL*) gene encoding only the PAZ domain and two RNaseIII domains (Figure 4A). The *mDCL* locus is not located near Pp *DCL1b*, as they reside on different chromosomes. mDCL is not an obvious member of any of the canonical four clades of plant DCL proteins, although its phylogenetic position was difficult to resolve (Figure 4A). The protozoan parasite *Giardia intestinalis* has been shown to produce a functional Dicer with a similarly minimal domain composition (Macrae et al., 2006). In addition, the ciliated protozoan *Tetrahymena thermophila* also produces a Dicer protein that lacks an N-terminal helicase domain (although it also lacks a PAZ domain); *T. thermophila DCL1* is required for accumulation of scan RNAs that direct programmed DNA deletion events (Malone et al., 2005; Mochizuki and Gorovsky, 2005). Rice (*Oryza sativa*) DCL2b has a similar truncated domain structure, and a *S. moellendorffii* DCL protein (429802) has a PAZ domain followed by a single RNaseIII domain (Figure 4A). Importantly, mDCL was basal to all four clades of plant DCLs (Figure 4A), while the Os DCL2b and Sm 429802 were clear recent duplicates of DCL2 and DCL3, respectively. We hypothesized that *mDCL* contributes to production of endogenous *P. patens* siRNAs. To test this hypothesis, we used homologous recombination to obtain two independent *mdcl* mutant lines (Supplemental Figure 3).

Heterochromatic siRNA Mutants and *mdcl* Mutants Have a Similar Accelerated Growth Phenotype

Previous analyses collectively indicated that *P. patens* has one homolog of the Arabidopsis Pol IV largest subunit (Pp *NRPD1*) and two homologs of the Pol V largest subunit (Pp *NPRE1a* and Pp *NRPE1b*) (Arif et al., 2013; Huang et al., 2015). A high density of multiple GW/WG/GWG motifs in the C-terminal domain is a characteristic of the Pol V, but not the Pol IV largest subunit (Haag and Pikaard, 2011). We found that Pp *NRPE1b*, but not Pp *NRPE1a*, had many C-terminal GW/WG/GWG motifs (Figure 4B). Pp *NRPE1a* is positioned around 600 kb away from Pp *NRPE1b*, suggestive of a recent tandem duplication. The Pp *NRPE1a* gene was previously suggested to be a Pol IV largest subunit homolog (Arif et al., 2013). Using homologous recombination, we obtained a single mutant line each for

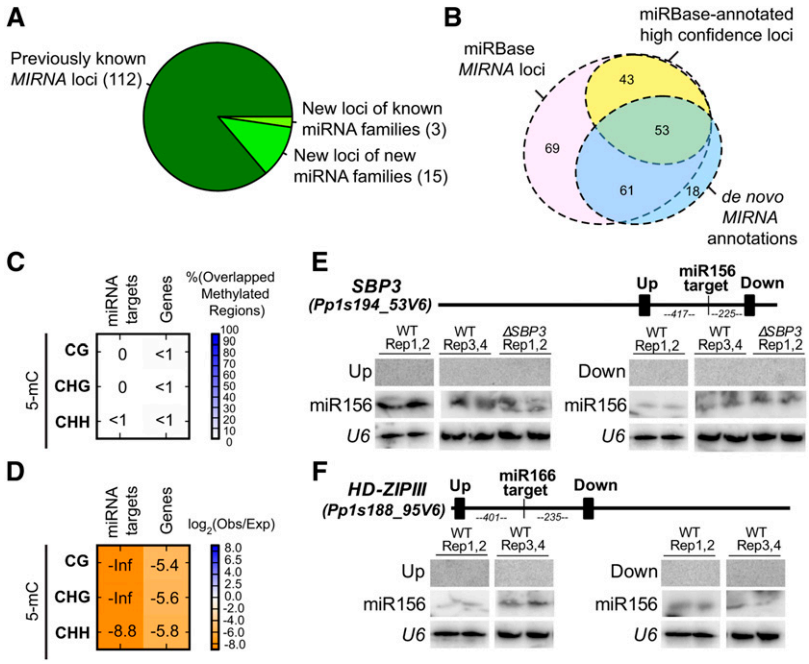

Figure 3. Refinement of *P. patens MIRNA* Annotations and Functions.

(A) Classification of *MIRNA* loci confidently identified in this study.
(B) Euler diagram comparing our de novo *MIRNA* annotations with previously annotated *P. patens MIRNA* loci from miRBase 21.
(C) Percentage overlaps of regions of dense DNA methylation with miRNA targets and *P. patens* genes. Calculated as in Figure 2A.
(D) Enrichment/depletion analysis of methylated regions of genome with miRNA targets and *P. patens* genes. Calculated as in Figure 2C.
(E) RNA gel blot of small RNAs surrounding miR156 target site in Pp *SBP3*. Filled rectangles on the gene schematic indicate probe positions. Up, upstream of target site; down, downstream of target site.
(F) RNA gel blot of small RNAs surrounding miR166 target site in *HD-ZIPIII*. Filled rectangles on the gene schematic indicate probe positions. Numbers indicate distances (nucleotides) between target sites and probed regions. Up, upstream of target site; down, downstream of target site.

Pp *nrpe1b* and Pp *nrpd1* (Supplemental Figures 4 and 5). Attempts to isolate a Pp *nrpe1a* mutant failed for unknown reasons.

P. patens contains *RDR* genes in the α and γ clades (Zong et al., 2009; Huang et al., 2015). Pp *rdr6* mutants have an accelerated juvenile-to-adult gametophyte transition phenotype and lose the accumulation of *trans*-acting siRNAs (Talmor-Neiman et al., 2006; Cho et al., 2008). Huang et al. (2015) referred to the only other *P. patens* member of the α clade as Pp *RDR1/2* because it is basal to the flowering plant *RDR1* and *RDR2* clades. Because our subsequent functional analysis demonstrated that the function of this gene is homologous to that of Arabidopsis *RDR2*, we refer to it here as simply Pp *RDR2*. It remains to be tested whether this locus also might perform *RDR1*-like functions. Two independent Pp *rdr2* mutant lines were created using homologous recombination (Supplemental Figure 6).

Expression levels in protonemata, as estimated by RNA-seq data (Chen et al., 2012), were moderate for all of the *P. patens* genes we studied, with the exception of Pp *NRPE1a*, for which we were unable to obtain a mutant (Figure 4C). This suggests that the protonematal stage of growth is a valid time point to assay for effect of these mutations on small RNA populations.

We previously observed that Pp *dcl3* mutants display an accelerated juvenile-to-adult transition in gametophyte growth (Cho et al., 2008). In flowering plants, *DCL3*, *RDR2*, Pol IV, and Pol V are known to collaborate in the heterochromatic siRNA pathway, so we hypothesized that Pp *rdr2*, Pp *nrpd1*, and Pp *nrpe1b* mutants would also display the same phenotype. We found that this was indeed the case (Figure 4D). We also found that *mdcl* plants had an accelerated juvenile-to-adult transition (Figure 4D), suggesting that *mDCL* also contributes to the heterochromatic siRNA pathway.

mDCL Promotes Accumulation of 23-Nucleotide RNAs from Heterochromatic siRNA Loci

We tested the hypothesis that the Pp *rdr2*, Pp *nrpd1*, Pp *nrpe1b*, and *mdcl* mutants affected 23- to 24-nucleotide siRNA accumulation by constructing and sequencing multiple small RNA-seq libraries from 10-d-old protonemata (Supplemental Table 1). Also included were Pp *dcl4* and Pp *rdr6* mutants (known to affect secondary siRNAs; Talmor-Neiman et al., 2006; Arif et al., 2012), and Pp *dcl3* mutants (which our previous analysis implicated in 23- to 24-nucleotide siRNA accumulation; Cho et al., 2008). All mutants were represented by two to four biological replicates (Figure 5A; Supplemental Table 1).

None of the mutants examined had significant effects on the *MIRNA* population (Figure 5). At 20- to 22-nucleotide siRNA loci,

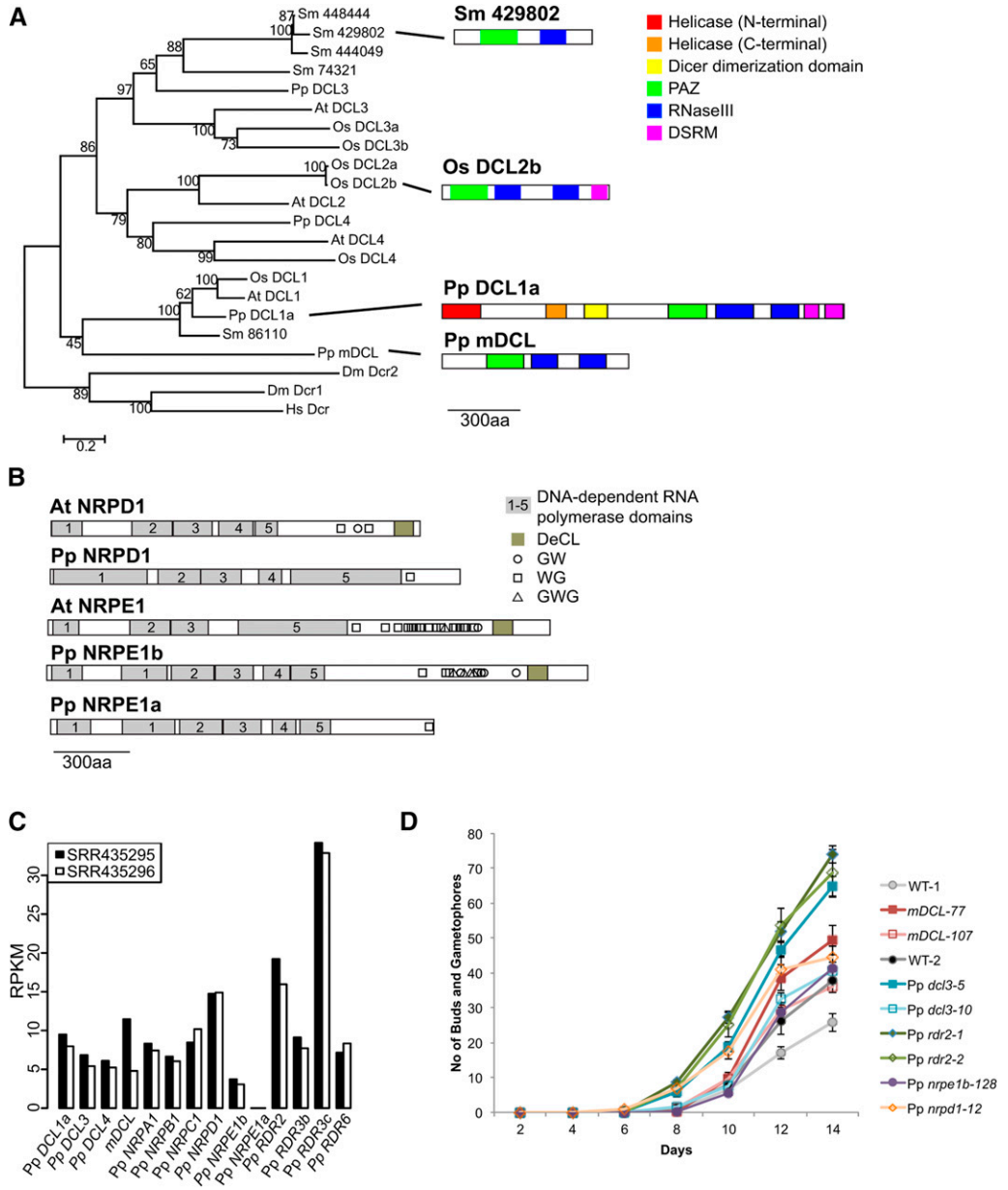

Figure 4. Analysis of *P. patens* Small RNA Biogenesis Genes and Their Mutant Phenotypes.

(A) Phylogenetic analysis of DCL proteins. At, *Arabidopsis thaliana*; Os, *Oryza sativa*; Sm, *Selaginella moellendorffii*; Pp: *P. patens*; Dm, *Drosophila melanogaster*; Hs, *Homo sapiens*. Numbers are bootstrap percentages from 1000 replicates. Scale bar indicates substitutions per site. Sidebar shows example domain structures of mDCL and two other proteins with a similar minimal domain structure, and Pp DCL1a was included as an example of a full-length DCL protein.
(B) Domain structures of Arabidopsis (At) and *P. patens* (Pp) largest subunits of DNA-dependent RNA polymerases. DeCL, DEFECTIVE CHLOROPLASTS AND LEAVES domain.
(C) mRNA accumulation for the indicated genes in protonemata according to RNA-seq data from the indicated accessions. RPKM, reads per kilobase per million.
(D) Rates of bud and gametophore production. Seven-day-old protonemal tissues were inoculated on BCD media, and the total numbers of buds and gametophores were counted every 2 d. Points show means and whiskers show standard errors of the means from 12 replicates.

the only significant difference in overall abundance was an increase in the Pp *nrpe1b* mutant (Figure 5A). However, when examining size distributions, Pp *rdr6* mutants clearly lost 21-nucleotide RNAs, but not 22-nucleotide RNAs, from the 20- to 22-nucleotide loci (Figure 5B). We noted that none of the Dicer-like mutants tested affected the levels of small RNAs from 20- to 22-nucleotide siRNA loci. Pp *DCL1a* was the only *P. patens dcl* mutant not examined in our study, and we suspect that many of these loci are Pp *DCL1*a dependent. Several of the mutants had major effects on small RNAs from 23- to 24-nucleotide

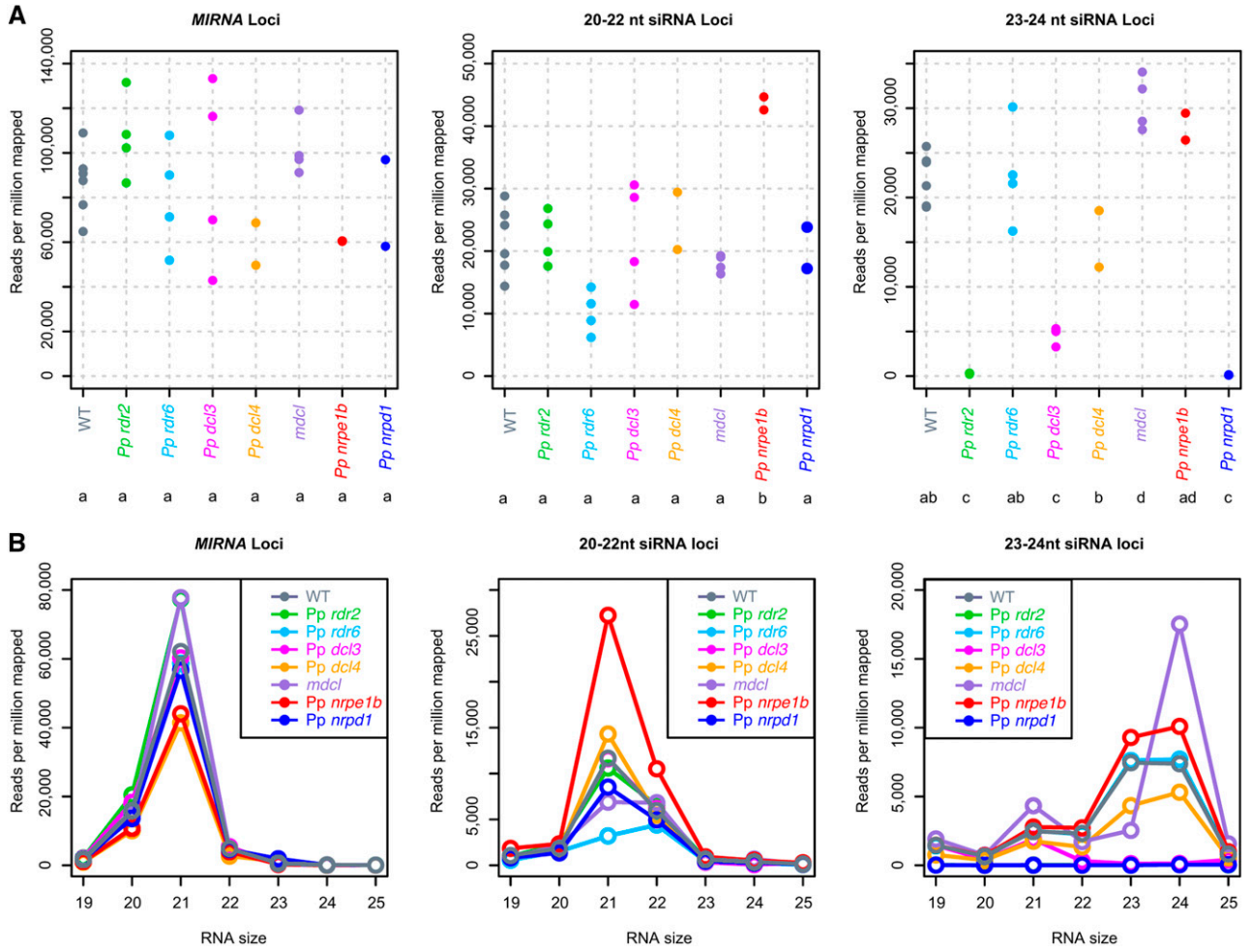

Figure 5. *mDCL* Promotes 23-Nucleotide RNA Accumulation and Represses 24-Nucleotide RNA Accumulation at Heterochromatic siRNA Loci.

(A) Overall small RNA abundance at *MIRNA*, 20- to 22-nucleotide siRNA loci, and 23- to 24-nucleotide siRNA loci. Each dot represents a biological replicate small RNA-seq sample. Genotypes sharing a letter have means that are not significantly different (Tukey's honestly significant difference test, $\alpha = 0.05$).

(B) Small RNA abundance by size within *MIRNA* loci, 20- to 22-nucleotide siRNA loci, and 23- to 24-nucleotide siRNA loci for the indicated genotypes. Reads for all biological replicates within each genotype were summed and converted to reads per million mapped.

siRNA loci. Pp *rdr2*, Pp *nrpd1*, and Pp *dcl3* mutants had the most severe effects; siRNAs of all sizes were essentially absent from 23- to 24-nucleotide siRNA loci in the Pp *rdr2* and Pp *nrpd1* plants, while only 21-nucleotide RNAs remained in Pp *dcl3* (Figure 5B). The specific loss of 23- to 24-nucleotide RNAs, but not 21-nucleotide RNAs, in the Pp *dcl3* background is consistent with our earlier smaller scale observations (Cho et al., 2008). Pp *nrpe1b* and Pp *rdr6* mutants did not have strong changes in overall RNA accumulation levels from 23- to 24-nucleotide siRNA loci (Figure 5). *mdcl* mutants had unique alterations in their small RNA profiles at 23- to 24-nucleotide siRNA loci; the levels of 23-nucleotide siRNAs were decreased, but the levels of 21-nucleotide, and especially 24-nucleotide, siRNAs were increased (Figure 5B). We conclude that *mDCL* affects the heterochromatic siRNA pathway by promoting the production of 23-nucleotide siRNAs at the expense of 21- and 24-nucleotide siRNAs.

Differential Expression Analysis Reveals Distinct Subgroups of Heterochromatic siRNA Loci

A differential expression analysis was performed by tallying small RNA alignments of all sizes from each library within each of our annotated *DCL*-derived small RNA loci. A multidimensional scaling plot of these data was prepared to illustrate overall differences in small RNA accumulation between each of the samples (Figure 6). Biological replicates for each genotype were generally consistent with each other, indicated by their tight groupings on the multidimensional scaling plot (Figure 6A). Pp *rdr6*, Pp *dcl4*, *mdcl*, and Pp *nrpe1b* mutants clustered closely

with the wild type, while Pp *rdr2* and Pp *nrpd1* formed a second cluster of libraries distinct from the wild-type and from all of the other mutants (Figure 6A). A third, looser cluster was formed by the Pp *dcl3* mutants.

Loci were considered differentially expressed (DE) in a particular mutant if they had at least a 2-fold change compared with the wild type at a false discovery rate of <0.01 (Supplemental Data Set 7). Very few DE loci were found in Pp *dcl4* and Pp *rdr6* mutants, indicating that the secondary siRNA pathway does not make a major contribution to most of the endogenous small RNA loci under study (Figure 6B). Large numbers of downregulated 23- to 24-nucleotide siRNA loci were found in Pp *rdr2* and Pp *nrpd1* mutants (Figure 6B). A much smaller number of downregulated 23- to 24-nucleotide siRNA loci were apparent in Pp *dcl3* and Pp *nrpe1b* mutants (Figure 6B). The modest numbers of upregulated loci observed in Pp *dcl3*, Pp *nrpd1*, and Pp *rdr2* mutants were mostly *MIRNA*s (Figure 6B). It is possible that the heterochromatic siRNAs dependent on Pp *dcl3*, Pp *nrpd1*, and Pp *rdr2* compete with miRNA accumulation. Alternatively, because small RNA-seq quantification is proportional rather than absolute, small RNAs from these loci may appear upregulated only because of the gross absence of 23- to 24-nucleotide siRNAs in these samples. Interestingly, relatively small numbers of 23- to 24-nucleotide siRNA loci were upregulated in the Pp *nrpe1b* mutant (Figure 6B), suggesting the existence of distinct subsets of heterochromatic siRNA loci. This is consistent with the effect of Arabidopsis Pol V on only a subset of heterochromatic siRNAs (Mosher et al. 2008). Finally, 23- to 24-nucleotide siRNA loci did not appear as DE in *mdcl* mutants because decreased accumulation of 23 nucleotide RNAs were compensated for by the increased accumulation of 24-nucleotide RNAs, resulting in similar total small RNA accumulations to that of the wild type (Figures 5B and 6B).

We next integrated DE calls for loci between the various mutants. We plotted and analyzed the 10 most common patterns of loci for the four mutants of major effect (Figure 6C). Pp *rdr6*, Pp *dcl4*, and *mdcl* were not involved in any of the top 10 patterns, so were omitted from the figure. Loci downregulated

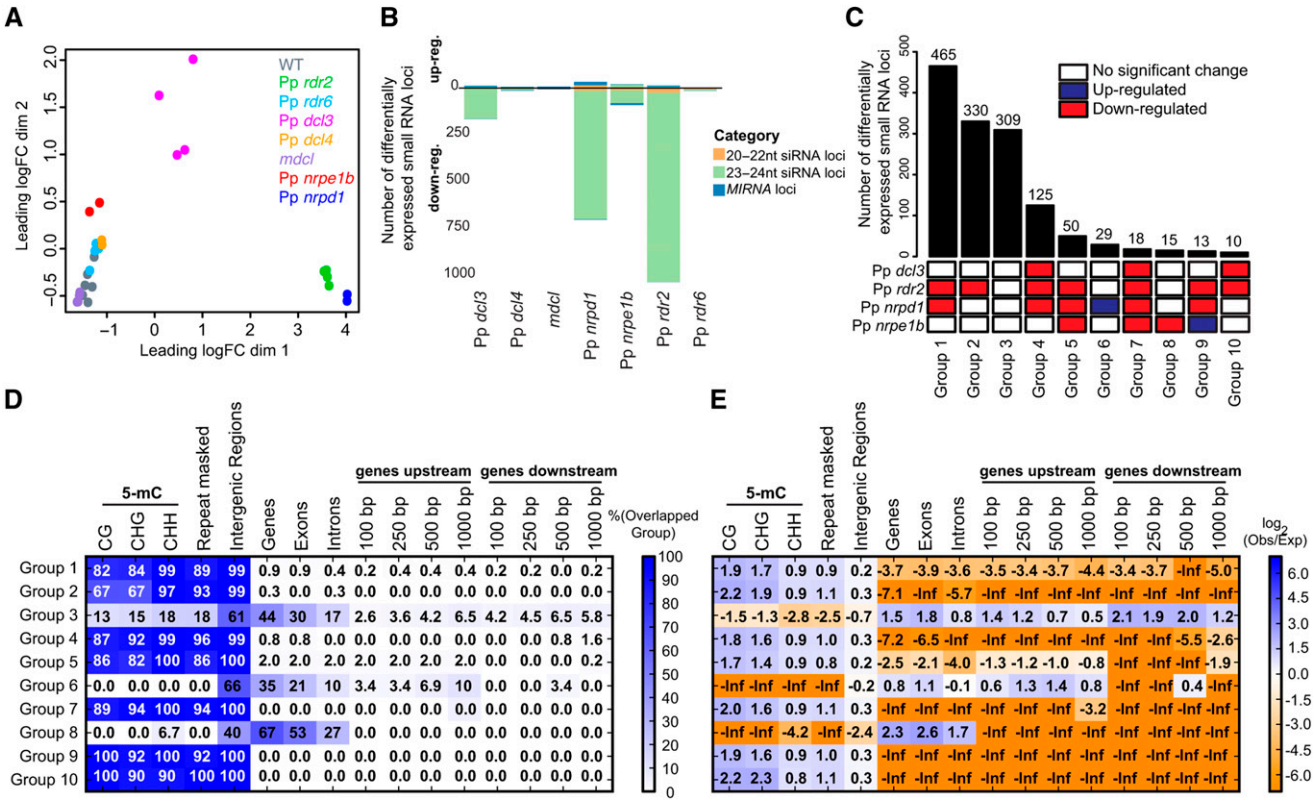

Figure 6. Differential Expression Analysis of *P. patens* Small RNAs in Mutants.

(A) Multidimensional scaling plot showing the overall relationship between each mutant and wild-type biological replicate small RNA-seq library. Leading fold change (FC) is the (root mean square) average of the largest absolute $\log_2$ fold changes between each pair of samples.

(B) Numbers of differentially downregulated or upregulated small RNA loci in each of the indicated mutants compared with the wild type. Differential expression for a locus is defined as with at least 2-fold-change with a false discovery rate of <0.01.

(C) Numbers of differentially expressed loci (bar chart; upper panel) represented by different mutant combinations (heat map; lower panel).

(D) Observed overlap/expected overlap ratios for different mutant groups defined in **(C)** relative to various genomic features. Calculated as in Figure 2C.

(E) Overlap percentage for mutant groups defined in **(C)** relative to various genomic features. Calculated as in Figure 2A. Repeat-masked: repeats of various types as annotated by the Joint Genome Initiative genome annotation.

in both Pp *rdr2* and Pp *nrpd1* mutants were most numerous (Group 1, Figure 6C). Group 2 loci were downregulated only in the Pp *rdr2* mutant, while group 4 was composed of loci downregulated in Pp *dcl3*, Pp *rdr2*, and Pp *nrpd1* (Figure 6C). Group 5 loci were downregulated in Pp *rdr2*, Pp *nrpd1*, and Pp *nrpe1b*. Except for groups 6 and 9, the remainder of the most common patterns were loci that were downregulated in one or more of the Pp *dcl3*, Pp *rdr2*, Pp *nrpd1*, and Pp *nrpe1b* mutants. To sum up, the DE patterns of mutants whose direct homologs in Arabidopsis are involved in the canonical Pol IV RdDM pathway tend to be similar.

Pp *nrpe1b* mutants had an interesting pattern of DE loci. Fifteen loci were downregulated solely in this mutant while not significantly changed in the other three mutants (Group 8, Figure 6C). Thirteen loci were upregulated in Pp *nrpe1b* mutants but downregulated in Pp *rdr2* and Pp *nrpd1* mutants (Group 9, Figure 6C). Thus, there appear to be distinct subsets of heterochromatic siRNA loci uniquely affected by Pp *NRPE1b*. Pp *nrpd1* mutants were also interesting, with 29 loci upregulated only in Pp *nrpd1* mutants but not significantly changed in the other three mutants (Group 6, Figure 6C). Pp *NRPD1* therefore negatively regulates a unique subset of heterochromatic siRNA loci in terms of overall small RNA abundance. Co-occupancy analysis of the loci in these groups of interest relative to general genomic features revealed distinct patterns (Figures 6D and 6E). First, loci that were not DE in any of the mutants (Group 3) seemed to overlap with genes and gene-proximal regions and were depleted in regions characteristic of heterochromatic siRNAs. Second, loci that were upregulated only in Pp *nrpd1* (Group 6) and loci that were solely downregulated in Pp *nrpe1b* (Group 8) mutants were depleted for overlaps with 5-mC, repeats, and intergenic regions. Pp *nrpe1b*-dependent loci (Group 8) were highly enriched in genes, while Pp *nrpd1*-dependent loci (Group 6) were associated with both genes and upstream of genes (Figures 6D and 6E). All of the other groups were enriched for overlaps with 5-mC and repeats and depleted for overlaps with genes and gene-proximal regions (Figures 6D and 6E).

P. patens Heterochromatic siRNAs Suppress Expression of LTR Retrotransposon-Related Sequences Despite Minimal Changes in DNA Methylation

To test whether loss of *P. patens* 23- to 24-nucleotide siRNAs affects 5-mC patterns, whole-genome shotgun sequencing of bisulfite converted DNA was performed from one wild-type specimen and one specimen each from both Pp *rdr2-1* and Pp *rdr2-2* mutant plants. Numerous PCR duplicates were observed in these libraries (Supplemental Table 2). After removing them, genomic coverage was very sparse (over 80% of Cs in the nuclear genome had no coverage) and biased toward repetitive regions (Supplemental Figures 7A and 7B). Bulk DNA methylation patterns in the nuclear genome were very similar between the wild type and the two Pp *RDR2* mutant specimens in all three sequence contexts (Supplemental Figure 7C). Mutation of *rdr2* caused no obvious changes in DNA methylation in the population of 23- to 24-nucleotide siRNA loci nor in any of the groups of differentially expressed loci from Figure 6 (Supplemental Figure 8). However, because of low coverage, groups 6 and 8 were not able to be analyzed.

Previously, we described two families of reverse transcriptase genes, *RT3* and *RT6*, from *P. patens* high-copy LTR retrotransposons that were silent in the wild type but expressed in the Pp *dcl3* mutant (Cho et al., 2008). The overall patterns of small RNA accumulation at these loci in the various mutants mirrored those of the 23- to 24-nucleotide siRNA loci (Figures 7A and 7B). At *RT3* loci, no strong changes in DNA methylation were observed in the Pp *rdr2* mutants (Figure 7C). However, at more than 75% of the *RT6* loci, there was a decrease in 5-mC in Pp *rdr2* mutants specifically in the CHG context (Figure 7C), suggesting that Pp *RDR2* is required to maintain wild-type levels of CHG methylation at many of these loci. Pp *rdr2* mutants have significantly increased accumulation of long RNAs from both *RT3* and *RT6* loci (Figure 7D). Pp *nrpd1* mutants have increased accumulation of long RNAs from *RT6*, but not *RT3* loci (Figure 7D). These results indicate that Pp *RDR2* and Pp *NRPD1* play a role in suppressing long RNA accumulation from these LTR retrotransposon-related loci. Overall, however, this analysis did not find strong evidence that Pp *RDR2*-dependent siRNAs are required to maintain most existing patterns of 5-mC.

DISCUSSION

We analyzed more than 100 million mapped small RNA-seq reads from wild-type *P. patens* and used these data to produce a comprehensive set of small RNA gene annotations. Setting aside degradation products that are unlikely to be part of the DCL/AGO regulatory system, most *P. patens* small RNA genes produce 23- to 24-nucleotide siRNAs. These loci are enriched for overlaps with repeats and regions of dense 5-mC and nearly always avoid protein-coding genes. The *P. patens* 23- to 24-nucleotide siRNA loci are also strongly dependent on Pp *RDR2*, Pp *NRPD1* (the presumed largest subunit of a Pol IV complex), and Pp *DCL3* for small RNA production. Altogether, these data lead us to conclude that *P. patens* uses a heterochromatic siRNA pathway fundamentally similar to that of flowering plants. Therefore, the potential absence of heterochromatic siRNAs in conifers (Dolgosheina et al., 2008; Morin et al., 2008) and lycophytes (Banks et al., 2011) could reflect secondary loss of the pathway in those specific lineages. However, more recent data show that, for conifers, endogenous 24-nucleotide siRNAs can be found, albeit sometimes in tissue-specific patterns (Nystedt et al., 2013; J. Zhang et al., 2013) or in unique lineages such as cycads and *Gingko* (Chávez Montes et al., 2014). Thus, we favor the hypothesis that, like miRNAs, heterochromatic siRNAs are a universal feature of land plant transcriptomes.

However, *P. patens* heterochromatic siRNAs do have some atypical features compared with those in flowering plants. Small RNA-seq samples from most wild-type tissues of most flowering plants are dominated by 24-nucleotide heterochromatic siRNAs. In contrast, heterochromatic siRNAs are weakly expressed in *P. patens* protonemata, where 21-nucleotide miRNA expression dominates the small RNA profile in terms of abundance. Also in contrast to flowering plants, whose heterochromatic siRNAs are mostly 24 nucleotides, *P. patens* heterochromatic siRNA loci produce a mixture of 23- and 24-nucleotide RNAs at nearly equal levels, with much lower levels of 21- and 22-nucleotide RNAs. Our genetic analysis indicates that the *mDCL* gene is

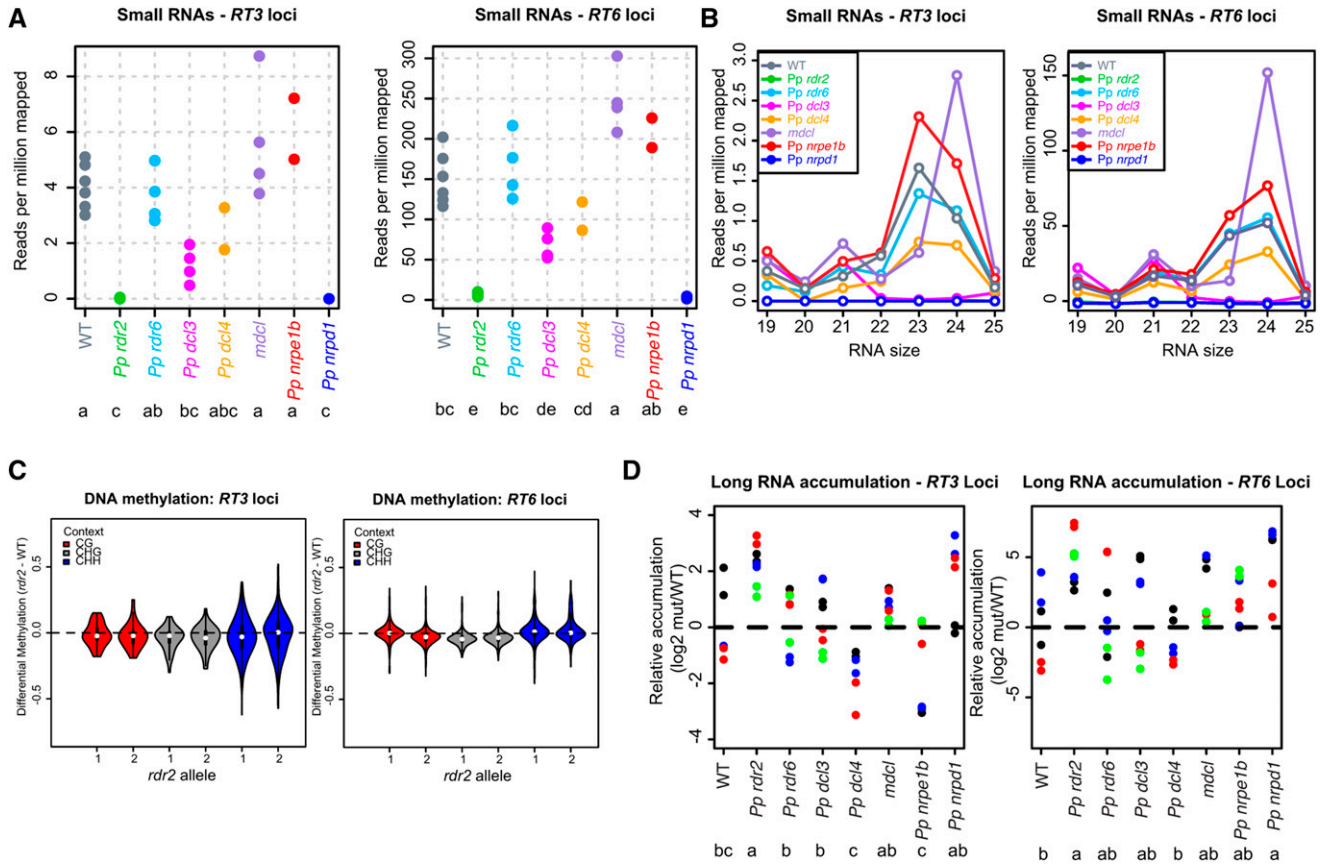

Figure 7. Effects of the *P. patens* Heterochromatic siRNA Pathway on the LTR Retrotransposon-Related Sequences *RT3* and *RT6*.

(A) Overall small RNA abundance at *RT3* and *RT6* loci. Each dot represents a biological replicate small RNA-seq sample. Genotypes sharing a letter have means that are not significantly different (Tukey's honestly significant difference test, $\alpha = 0.05$).

(B) Small RNA abundance by size within *RT3* loci and *RT6* loci for the indicated genotypes. Reads for all biological replicates within each genotype were summed and converted to reads per million mapped.

(C) Differential DNA methylation between the indicated Pp *rdr2* alleles and the wild type at *RT3* loci (left) and *RT6* loci (right). Violin plots show a Tukey box plot (line = median, box edges = 1st and 3rd quartiles, whiskers = 1.5 IQR) surrounded by a twinned kernel density plot to visually show the distribution of the data.

(D) Long RNA accumulation based on quantitative RT-PCR from *RT3* loci (left) and *RT6* loci (right). Dots of the same color represent different technical replicates of the same biological replicate. Genotypes sharing a letter have means that are not significantly different (Tukey's honestly significant difference test, $\alpha = 0.05$).

responsible specifically for 23-nucleotide siRNA accumulation from these loci; in *mdcl* mutants, 23-nucleotide RNAs are strongly reduced, while 24-nucleotide RNAs are strongly increased at heterochromatic siRNA loci. At the same loci, loss of Pp *DCL3* function eliminates all sizes of small RNA accumulation. We speculate that mDCL is dependent upon Pp DCL3 due to its lack of an N-terminal helicase domain. We also speculate that mDCL competes with Pp DCL3 for small RNA precursors produced by Pol IV and Pp RDR2. In *mdcl* mutants, Pp DCL3 processes the excess precursors to make mostly 24-nucleotide RNAs. In Pp *dcl3* mutants, mDCL cannot function, leading to the loss of both the *mDCL*-dependent 23-nucleotide and Pp DCL3-dependent 24-nucleotide RNAs. Further investigation is required to test this hypothesis. There are precedents for competition in small RNA size classes in plants: Mutation of maize (*Zea mays*) *mop1*, an *RDR2* homolog, reduces 24-nucleotide siRNA accumulation but enhances 22-nucleotide siRNA accumulation (Nobuta et al., 2008). Also, there are known Arabidopsis loci where multiple DCLs engage the same template, such as the inverted repeat locus *IR71* (Dunoyer et al., 2010). We find proteins with a mDCL-like arrangement of domains in *S. moellendorffii* and rice, but neither are clear mDCL homologs; instead, they are recent duplications of *DCL3* clade and *DCL2* clade genes, respectively (Figure 4A). This suggests that *mDCL* genes might arise frequently during plant evolution.

Our genetic analyses show that *P. patens* expresses heterochromatic siRNAs that have a largely similar biogenesis pathway as in flowering plants. Therefore, the most parsimonious scenario is that, as for miRNAs, the heterochromatic siRNA pathway is an ancestral trait that was present in the last common ancestor

of bryophytes and all other subsequently diverged lineages of plants. The major differences are the relative levels of expression in vegetative tissue and the use of the novel *mDCL* gene to produce 23-nucleotide heterochromatic siRNAs in *P. patens*. We also suggest that *P. patens* miRNA functions may not be as unusual as has previously been suggested (Khraiwesh et al., 2010); we find no evidence that *P. patens* miRNAs spawn abundant secondary siRNAs from protein-coding target mRNAs nor direct 5-mC deposition at target chromatin. It remains possible that these miRNA functions occur under specific conditions not represented in our study. Finally, our publically available and browsable annotations of *P. patens* small RNA genes (http://plantsmallrnagenes.psu.edu/physcomitrella_patens) provide a comprehensive and useful resource for further study of all classes of small RNAs in this model organism.

METHODS

Small RNA-seq and Reference Annotation of Wild-Type *P. patens* Small RNA Genes

Total RNA was extracted using the miRNeasy Mini kit (Qiagen) per the manufacturer's instructions from 10-d-old *Physcomitrella patens* protonemata grown on cellophane-overlaid BCD medium (Ashton and Cove, 1977) supplemented with 5 mM ammonium tartrate and cultured at 25°C, 16 h day/8 h night. Small RNA libraries were constructed using the TruSeq Small RNA kit (Illumina) per the manufacturer's instructions and sequenced on a HiSequation 2500 (Illumina) instrument using 50-nucleotide single-end runs. Small RNA-seq data from the wild-type libraries (Supplemental Table 1) were analyzed with ShortStack version 2.0.0 (Axtell, 2013b). First, each library was adapter trimmed and aligned to the reference genome (version 3.0 nuclear assembly from Phytozome v10.1; *Physcomitrella patens* v3.0, DOE-JGI, http://phytozome.jgi.doe.gov/pz/portal.html#!info?alias=Org_Ppatens; Rensing et al., 2008; Goodstein et al., 2012) combined with the plastid and mitochondrial genomes) using default butter version 0.0.3 settings with –adapter TGGAATTC. The alignments were then run with ShortStack mindepth 4 to find abundance of small RNAs at the de novo ShortStack-identified small RNA loci. Bedtools (Quinlan and Hall, 2010) was used to find shared clusters in six different wild-type libraries and then the output was filtered so that only regions that were present in at least 4 (out of 6) libraries were used to serve as the final reference small RNA locus boundaries. ShortStack-count mode under default settings was then used to find relative small RNA abundance on this reference list of de novo-identified small RNA loci for each wild-type and mutant library. Full results are listed in Supplemental Data Set 1, and the annotations are also hosted at http://plantsmallrnagenes.psu.edu/physcomitrella_patens. Raw wild-type small RNA-seq data, processed data, and alignments were deposited to the NCBI Gene Expression Omnibus (GEO) (GSE44900) and are also available at http://plantsmallrnagenes.psu.edu/physcomitrella_patens.

Co-Occupancy Analyses

Regions of dense 5-mC occupancy in the CG, CHG, and CHH contexts were calculated in 50-nucleotide intervals based on protonematal bisulfite-seq data from NCBI GEO accession GSM497264 (Zemach et al., 2010). A given 50-nucleotide interval was considered densely methylated in a particular context if there were more than six reads of all Cs in that context and more than a threshold percentage of those were unconverted (60% threshold for CG and CHG contexts; 20% threshold for CHH contexts). Repeat-masked regions were obtained from version 3.0 of the nuclear assembly from Phytozome v10.1 (*Physcomitrella patens* v3.0, DOE-JGI, http://phytozome.jgi.doe.gov/pz/portal.html#!info?alias=Org_Ppatens; Rensing et al., 2008; Goodstein et al., 2012). Intergenic, genic, exonic, intronic, gene upstream, and gene downstream locations were calculated based on version 3.0 of the transcriptome assembly gff3 file obtained from Phytozome 10.1. rRNA gene locations were based on regions of significant similarity (BLASTn e-value of $\leq$ 1E-10) to the rRNA consensus sequences. tRNA gene locations were based on genome-wide analysis with tRNAscan-SE version 1.3.1 under default parameters (Lowe and Eddy, 1997). Raw data for all of these annotations are retrievable and browsable at plantsmallrnagenes.psu.edu/physcomitrella_patens/jbrowse/.

The absolute numbers of overlapping loci and the total of nonredundant overlapping nucleotides for each pairwise comparison of feature types were calculated. Enrichment/depletion was calculated based on the ratio of the observed to the expected number of overlapping nucleotides. The expected number of overlapping nucleotides for any pairwise feature comparison is given by $E = (x/g) * (y/g) * g$, where E is the expected number of overlapping nucleotides under the null hypothesis of random location, x is the total number of nonredundant nucleotides for feature type 1, y is the total number of nonredundant nucleotides for feature type 2, and g is the total genome size.

miRNA and miRNA Target Analyses

MIRNA hairpin sequences and mature miRNA sequences identified by our de novo annotation effort were compared with the prior annotations in miRBase 21. The 18 loci that had not been previously annotated were registered with miRBase. We also used miRBase's "confidence" community annotation system (Kozomara and Griffiths-Jones, 2014) to up-vote and comment on the existing annotations. A set of 42 high-confidence miRNA target genes was curated from Addo-Quaye et al. (2009) (Supplemental Data Set 5) and compared with the 5-mC data (see above for processing methods) from Zemach et al. (2010).

Small RNA Gel Blots

Small RNA gel blots were performed as described (Cho et al., 2012) with modification. Total RNAs from 10-d-old samples were extracted using Tri-Reagent (Sigma-Aldrich), and small RNAs were fractionated as described (Pall and Hamilton, 2008). Twenty micrograms of total RNAs was separated on 20% PAGE gel, transblotted onto the Hybond X membrane (GE Healthcare), and cross-linked using 1-ethyl-3-(3-dimethylamonipropyl) carbodiimide (Pall and Hamilton, 2008). Probes were independently labeled with T4 polynucleotide kinase (New England Biolabs) and mixed before hybridization. Hybridization, washing, and detection were performed as described (Cho et al., 2012). The probe sequences are listed in Supplemental Table 3.

Phylogenetic Analysis

DCL protein sequences were trimmed to include only the C-terminal portions, beginning 50 residues before the PAZ domain. Sequence alignments of trimmed DCL proteins were generated using MUSCLE in the MEGA5 software (Tamura et al., 2011) with default parameters (Supplemental Data Set 8) and used for phylogenetic analysis (MEGA5) using the maximum likelihood method based on the JTT matrix-based model with uniform rates. All positions with alignment gaps were used. The tree with the highest log likelihood was shown, and topology reliability was checked using bootstrap analysis with 1000 replicates.

Construction of Vectors

For the construction of knockout vectors, two ~1-kb regions 5′ and 3′ from the open reading frame of desired genes were amplified using specific primer sets (Supplemental Table 3) and inserted into the pUQ vector (Cho et al., 2008) as previously described (Cho et al., 2012).

DNA Gel Blot Analysis

Genomic DNAs were extracted using a Phytopure DNA Extraction kit (GE Healthcare). For DNA gel blot analysis, the *Bgl*II-digested genomic DNAs of *mdcl* and Pp *rdr2* were blotted onto a Hybond NX nylon membrane (GE Healthcare) and hybridized following a standard protocol (Sambrook and Russell, 2001). For a probe, PCR-amplified *hptII* fragment was radiolabeled with [α-^{32}P]dCTP using an NEblot Kit (New England Biolabs) per the manufacturer's instructions.

RT-PCR

Total RNAs were extracted from 10-d-old protonemata using the miRNeasy Mini kit (Qiagen). RT-PCR reactions were performed as previously described (Cho et al., 2012). Primer sequences are listed in Supplemental Table 3.

Differential Expression Analysis

Small RNA-seq samples from the various mutants (Supplemental Table 1) were trimmed (–adapter TGGAATTC), aligned to the version 3.0 genome (including plastid and mitochondrial genomes), and analyzed using ShortStack version 2.0.0 in count mode using the wild-type de novo small RNA gene annotations as the–count file. Counts from separate sequencing runs of the same libraries were combined (Supplemental Table 1) and used for differential expression analysis with the R package edgeR (Robinson et al., 2010). Libraries were normalized with the "calcNormFactors" function and analyzed with the "exactTest" function analysis for each mutant in comparison with the wild type. DE genes at a 1% false discovery rate were retrieved using the "decideTestsDGE" function and further filtered to retain only those with 2-fold or greater deviation from the wild type. Supplemental Data Set 7 contains the full details and results of these analyses.

Whole-Genome Bisulfite Sequencing

Library preparation was essentially as described by Hsieh et al. (2009). In brief, total genomic DNA was isolated from 10-d-old protonemata cultivated on BCDA media from three samples: the wild type (Gransden 2004 isolate), Pp *rdr2-1*, and Pp *rdr2-2* plants. DNA was isolated using DNeasy Plant Mini Kit (Qiagen) sheared by sonication to fragments of 350 to 850 bp, repaired using NEBNext End Repair Module protocol, purified using QIAquick PCR purification kit, and then ligated to custom Illumina paired-end adapters (sequencing primer A and sequencing primer B) that were synthesized with 5-methyl modifications on each cytosine position (Supplemental Table 3). The library was then treated with bisulfite with the Qiagen EpiTect Bisulfite kit, followed by 26 cycles of PCR amplification using Illumina PE PCR Primer A and Illumina PE PCR Primer B (Supplemental Table 3) and paired-end sequencing (100 $\times$ 100 nucleotides) on an Illumina GAIIx sequencing instrument.

Raw FASTQ data were processed to remove 3′ adapters and for quality using cutadapt version 1.8.1 (Martin, 2011) using nondefault settings: -O 1,–max-n 2, -q 20, -m 30, -a AGATCGGAAGAGCG, -A AGATCGGAAGAGCG. These trimmed FASTQ files were further processed with a perl script (Supplemental Data Set 9, script 1) that converts all Cs in the first mate set to Ts and all of the Gs in the second mate set to As, in both bases tracking the conversions by modifying the names of the reads. After this conversion, any mate-pair where one or more of the mates had a homopolymeric stretch of 20 or more was discarded, and the converted mates output to FASTA-formatted files. The reference genome (consisting of the plastid genome, the mitochondrial genome, and the version 3.0 nuclear genome from Phytozome 10; http://phytozome.jgi.doe.gov/pz/portal.html#!info?alias=Org_Ppatens; Rensing et al., 2008; Goodstein et al., 2012) was processed with a perl script (Supplemental Data Set 9, script 2) that makes two copies of each chromosome: one representing a fully converted top strand in which all Cs are converted to Ts, and a second representing the reverse complement of the bottom strand in which all Gs and converted to As. In the process, a large table documenting the positions of every C on both strands of the genome is created. The converted genome was then indexed using bowtie2-build (version 2.2.4; Langmead and Salzberg, 2012) under default parameters. The converted mate-paired read sets were then aligned to the converted genome using bowtie2 (version 2.2.5; Langmead and Salzberg, 2012) with nondefault settings -f, -X 800,–no-discordant,–no-mixed, -p 6 -D 30, -R 6, and –non-deterministic. The resulting SAM streams were piped through sequential samtools (version 1.2; Li et al., 2009) view and sort commands to create coordinate-sorted BAM alignment files. Fragments resulting from PCR duplication were defined as those sharing a common left end and flagged by setting bit 1024 in the SAM FLAG field using a perl script (Supplemental Data Set 9, script 3). The BAM files were then filtered using samtools view (version 1.2; Li et al., 2009) with options -b, -f 3, -F 1028, which outputs only alignments from concordantly mapped mate-pairs that are not flagged as PCR duplicates.

Using another perl script (Supplemental Data Set 8, script 4), along with the large table of genome-wide C positions (see above), the frequencies of converted and nonconverted Cs at each position in the genome were calculated and output into large tables. This analysis avoided "double-counting" information for positions that were covered by both mates of a mate-pair. All subsequent summaries and analyses of the results were based on analysis of these tables. Analyses of specific loci or 100-nucleotide genomic bins required a minimum number of reads covering Cs of 10 in each of the three libraries. Violin plots were produced in R (version 3.2.0) using vioplot (package version 0.2). The plots show a Tukey box plot (line = median, box edges = 1st and 3rd quartiles, whiskers = 1.5 IQR) surrounded by a twinned kernel density plot to visually show the distribution of the data.

Analyses of *RT3* and *RT6* Loci

RT3 and *RT6* loci were defined based on degenerate oligos first described by Cho et al. (2008) (Supplemental Table 3). The locations of *RT3* and *RT6* loci in the version 3.0 nuclear genome were determined by searching for all cases where exact matches to any permutation of the forward and any permutation of the reverse oligo were within 500 nucleotides of each in the opposite orientation. Lists of these loci are in Supplemental Data Sets 10 and 11. These lists were then compared with small RNA and bisulfite-seq data. Quantitative RT-PCR of these loci was performed from RNA samples extracted from 10-d-old protonemata (using the Qiagen miRNeasy Mini kit). cDNA was synthesized using Applied Biosystems High Capacity cDNA kit [mixture of oligo(dT) and random primers], amplified with Quantitect SYBR-Green master mix (Qiagen), and analyzed on an Applied Biosystems StepOne Plus real-time PCR system. Accumulation, relative to the control amplicon Pp *EF1-*α, was calculated and normalized for PCR efficiencies. The mean of the wild-type samples was set to one. Oligos are listed in Supplemental Table 3.

Accession Numbers

cDNA sequences for *mDCL*, Pp *NRPE1a*, and Pp *NRPE1b* have been deposited to NCBI under accession numbers KF179046, KF908783, and KF908782, respectively. Small RNA-seq data have been deposited to NCBI GEO under accession numbers GSE44900 (wild type) and GSE51419 (mutants). Bisulfite-seq data have been deposited at the Sequence Read Archive under accession numbers SRR2013850 (wild type), SRR2013877 (Pp *rdr2-1*), and SRR2013879 (Pp *rdr2-2*). The full set of *P. patens* small RNA gene annotations and associated data are also available and browsable at http://plantsmallrnagenes.psu.edu/physcomitrella_patens. Other accession numbers are as follows: At DCL1

(At1g01040), At DCL2 (At3g03300), At DCL3 (At3g43920), At DCL4 (At5g20320), Pp DCL1a (ABV31244.1), Pp DCL1b (DQ675601), Pp DCL3 (ABV31245), Pp DCL4 (EF670438), mDCL (KF179046), Os DCL1 (Os03g02970), Os DCL2a (Os03g38740), Os DCL2b (Os09g14610), Os DCL3a (Os01g68120), Os DCL3b/5 (Os10g34430), Os DCL4 (Os04g43050), Hs Dcr (Uniprot Q9UPY3), Dm Dcr1 (FlyBase FBgn0039016), and Dm Dcr2 (FlyBase FBgn0034246). *Selaginella moellendorffii* accession numbers are given in Figure 4A.

Supplemental Data

Supplemental Figure 1. Nucleotide frequencies of *Physcomitrella patens* small RNAs for each position.

Supplemental Figure 2. Discrepancies in Pp *DCL1b* annotations.

Supplemental Figure 3. Targeted knockout of *mDCL*.

Supplemental Figure 4. Targeted knockout of Pp *NRPE1b*.

Supplemental Figure 5. Targeted knockout of Pp *NRPD1*.

Supplemental Figure 6. Targeted knockout of Pp *RDR2*.

Supplemental Figure 7. Overview of bisulfite-seq libraries.

Supplemental Figure 8. Analysis of DNA methylation at 23- to 24-nucleotide siRNA loci in Pp *rdr2* mutants.

Supplemental Table 1. *Physcomitrella patens* small RNA-seq libraries.

Supplemental Table 2. Summary of bisulfite-seq libraries.

Supplemental Table 3. Oligonucleotide sequences used in this study.

Supplemental Data Set 1. *P. patens* small RNA-producing loci.

Supplemental Data Set 2. Text-based alignments of 130 *P. patens MIRNA* loci.

Supplemental Data Set 3. Summary of ShortStack-annotated miRNAs.

Supplemental Data Set 4. All miRBase loci and overlapping ShortStack loci.

Supplemental Data Set 5. Degradome-validated *P. patens* miRNA target genes and overlapping ShortStack small RNA loci.

Supplemental Data Set 6. Inferred mRNA sequence of Pp *DCL1b* from RNA-seq data.

Supplemental Data Set 7. Differential expression analysis details.

Supplemental Data Set 8. Alignment of DCL proteins used for phylogenetic analysis.

Supplemental Data Set 9. Perl scripts used for processing of bisulfite-seq data.

Supplemental Data Set 10. List of Pp *RT3* loci (version 3.0 nuclear genome).

Supplemental Data Set 11. List of Pp *RT6* loci (version 3.0 nuclear genome).

ACKNOWLEDGMENTS

We thank Tzahi Arazi for the gift of Pp *rdr6* mutant plants, Wolfgang Frank for the gift of Pp *dcl4* mutant plants, Brian Gregory for helpful discussions on this work and pilot small RNA-seq experiments, and Craig Praul and his colleagues at the Huck Institutes Genomics Core Facility for small RNA sequencing. Purchase of the Core Facility Illumina HiSeq 2500 instrument was supported by National Science Foundation Award 1229046 to M.J.A. This work was supported by grants from the Searle Scholars Program and NIH-NIGMS (R01-GM084051) to M.J.A.

AUTHOR CONTRIBUTIONS

C.C. and M.J.A. analyzed small RNA-seq data and wrote the article with input from all authors. S.H.C. generated *P. patens* mutants, characterized their phenotypes, and performed phylogenetic analyses. S.S. analyzed *MIRNA* annotations and functions. S.H.C. and Q.L. created small RNA-seq libraries. A.W. identified and cloned cDNAs for *P. patens* Pol IV and Pol V largest subunit homologs. M.J.A. conceived and supervised the project.

Received March 16, 2015; revised June 30, 2015; accepted July 7, 2015; published July 24, 2015.

REFERENCES

Addo-Quaye, C., Snyder, J.A., Park, Y.B., Li, Y.-F., Sunkar, R., and Axtell, M.J. (2009). Sliced microRNA targets and precise loop-first processing of MIR319 hairpins revealed by analysis of the Physcomitrella patens degradome. RNA **15:** 2112–2121.

Arazi, T., Talmor-Neiman, M., Stav, R., Riese, M., Huijser, P., and Baulcombe, D.C. (2005). Cloning and characterization of micro-RNAs from moss. Plant J. **43:** 837–848.

Arif, M.A., Fattash, I., Ma, Z., Cho, S.H., Beike, A.K., Reski, R., Axtell, M.J., and Frank, W. (2012). DICER-LIKE3 activity in *Physcomitrella patens* DICER-LIKE4 mutants causes severe developmental dysfunction and sterility. Mol. Plant **5:** 1281–1294.

Arif, M.A., Frank, W., and Khraiwesh, B. (2013). Role of RNA interference (RNAi) in the moss *Physcomitrella patens*. Int. J. Mol. Sci. **14:** 1516–1540.

Ashton, N.W., and Cove, D.J. (1977). The isolation and preliminary characterisation of auxotrophic and analogue resistant mutants of the moss, *Physcomitrella patens*. Mol. Gen. Genet. **154:** 87–95.

Axtell, M.J. (2013a). Classification and comparison of small RNAs from plants. Annu. Rev. Plant Biol. **64:** 137–159.

Axtell, M.J. (2013b). ShortStack: comprehensive annotation and quantification of small RNA genes. RNA **19:** 740–751.

Axtell, M.J., and Bartel, D.P. (2005). Antiquity of microRNAs and their targets in land plants. Plant Cell **17:** 1658–1673.

Axtell, M.J., Jan, C., Rajagopalan, R., and Bartel, D.P. (2006). A two-hit trigger for siRNA biogenesis in plants. Cell **127:** 565–577.

Axtell, M.J., Snyder, J.A., and Bartel, D.P. (2007). Common functions for diverse small RNAs of land plants. Plant Cell **19:** 1750–1769.

Banks, J.A., et al. (2011). The Selaginella genome identifies genetic changes associated with the evolution of vascular plants. Science **332:** 960–963.

Chávez Montes, R.A., de Fátima Rosas-Cárdenas, F., De Paoli, E., Accerbi, M., Rymarquis, L.A., Mahalingam, G., Marsch-Martínez, N., Meyers, B.C., Green, P.J., and de Folter, S. (2014). Sample sequencing of vascular plants demonstrates widespread conservation and divergence of microRNAs. Nat. Commun. **5:** 3722.

Chen, Y.-R., Su, Y.S., and Tu, S.-L. (2012). Distinct phytochrome actions in nonvascular plants revealed by targeted inactivation of phytobilin biosynthesis. Proc. Natl. Acad. Sci. USA **109:** 8310–8315.

Cho, S.H., Addo-Quaye, C., Coruh, C., Arif, M.A., Ma, Z., Frank, W., and Axtell, M.J. (2008). *Physcomitrella patens* DCL3 is required for 22-24 nt siRNA accumulation, suppression of retrotransposon-derived transcripts, and normal development. PLoS Genet. **4:** e1000314.

Cho, S.H., Coruh, C., and Axtell, M.J. (2012). miR156 and miR390 regulate tasiRNA accumulation and developmental timing in *Physcomitrella patens*. Plant Cell **24:** 4837–4849.

Coruh, C., Shahid, S., and Axtell, M.J. (2014). Seeing the forest for the trees: annotating small RNA producing genes in plants. Curr. Opin. Plant Biol. **18:** 87–95.

Daxinger, L., Kanno, T., Bucher, E., van der Winden, J., Naumann, U., Matzke, A.J.M., and Matzke, M. (2009). A stepwise pathway for biogenesis of 24-nt secondary siRNAs and spreading of DNA methylation. EMBO J. **28:** 48–57.

Dolgosheina, E.V., Morin, R.D., Aksay, G., Sahinalp, S.C., Magrini, V., Mardis, E.R., Mattsson, J., and Unrau, P.J. (2008). Conifers have a unique small RNA silencing signature. RNA **14:** 1508–1515.

Dunoyer, P., Brosnan, C.A., Schott, G., Wang, Y., Jay, F., Alioua, A., Himber, C., and Voinnet, O. (2010). An endogenous, systemic RNAi pathway in plants. EMBO J. **29:** 1699–1712.

Fattash, I., Voss, B., Reski, R., Hess, W.R., and Frank, W. (2007). Evidence for the rapid expansion of microRNA-mediated regulation in early land plant evolution. BMC Plant Biol. **7:** 13.

Goodstein, D.M., Shu, S., Howson, R., Neupane, R., Hayes, R.D., Fazo, J., Mitros, T., Dirks, W., Hellsten, U., Putnam, N., and Rokhsar, D.S. (2012). Phytozome: a comparative platform for green plant genomics. Nucleic Acids Res. **40:** D1178–D1186.

Haag, J.R., and Pikaard, C.S. (2011). Multisubunit RNA polymerases IV and V: purveyors of non-coding RNA for plant gene silencing. Nat. Rev. Mol. Cell Biol. **12:** 483–492.

Hsieh, T.-F., Ibarra, C.A., Silva, P., Zemach, A., Eshed-Williams, L., Fischer, R.L., and Zilberman, D. (2009). Genome-wide demethylation of *Arabidopsis* endosperm. Science **324:** 1451–1454.

Huang, Y., Kendall, T., Forsythe, E.S., Dorantes-Acosta, A., Li, S., Caballero-Pérez, J., Chen, X., Arteaga-Vázquez, M., Beilstein, M.A., and Mosher, R.A. (2015). Ancient origin and recent innovations of RNA polymerase IV and V. Mol. Biol. Evol. **32:** 1788–1799.

Khraiwesh, B., Arif, M.A., Seumel, G.I., Ossowski, S., Weigel, D., Reski, R., and Frank, W. (2010). Transcriptional control of gene expression by microRNAs. Cell **140:** 111–122.

Kozomara, A., and Griffiths-Jones, S. (2014). miRBase: annotating high confidence microRNAs using deep sequencing data. Nucleic Acids Res. **42:** D68–D73.

Langmead, B., and Salzberg, S.L. (2012). Fast gapped-read alignment with Bowtie 2. Nat. Methods **9:** 357–359.

Law, J.A., Du, J., Hale, C.J., Feng, S., Krajewski, K., Palanca, A.M. S., Strahl, B.D., Patel, D.J., and Jacobsen, S.E. (2013). Polymerase IV occupancy at RNA-directed DNA methylation sites requires SHH1. Nature **498:** 385–389.

Li, H., Handsaker, B., Wysoker, A., Fennell, T., Ruan, J., Homer, N., Marth, G., Abecasis, G., and Durbin, R.; 1000 Genome Project Data Processing Subgroup (2009). The sequence alignment/map format and SAMtools. Bioinformatics **25:** 2078–2079.

Lippman, Z., and Martienssen, R. (2004). The role of RNA interference in heterochromatic silencing. Nature **431:** 364–370.

Lowe, T.M., and Eddy, S.R. (1997). tRNAscan-SE: a program for improved detection of transfer RNA genes in genomic sequence. Nucleic Acids Res. **25:** 955–964.

Macrae, I.J., Zhou, K., Li, F., Repic, A., Brooks, A.N., Cande, W.Z., Adams, P.D., and Doudna, J.A. (2006). Structural basis for double-stranded RNA processing by Dicer. Science **311:** 195–198.

Malone, C.D., Anderson, A.M., Motl, J.A., Rexer, C.H., and Chalker, D.L. (2005). Germ line transcripts are processed by a Dicer-like protein that is essential for developmentally programmed genome rearrangements of *Tetrahymena thermophila*. Mol. Cell. Biol. **25:** 9151–9164.

Margis, R., Fusaro, A.F., Smith, N.A., Curtin, S.J., Watson, J.M., Finnegan, E.J., and Waterhouse, P.M. (2006). The evolution and diversification of Dicers in plants. FEBS Lett. **580:** 2442–2450.

Martin, M. (2011). Cutadapt removes adapter sequences from high-throughput sequencing. EMBnet Journal **17:** 10–12.

Matzke, M.A., and Mosher, R.A. (2014). RNA-directed DNA methylation: an epigenetic pathway of increasing complexity. Nat. Rev. Genet. **15:** 394–408.

Mi, S., et al. (2008). Sorting of small RNAs into Arabidopsis argonaute complexes is directed by the 5′ terminal nucleotide. Cell **133:** 116–127.

Mochizuki, K., and Gorovsky, M.A. (2005). A Dicer-like protein in Tetrahymena has distinct functions in genome rearrangement, chromosome segregation, and meiotic prophase. Genes Dev. **19:** 77–89.

Morin, R.D., Aksay, G., Dolgosheina, E., Ebhardt, H.A., Magrini, V., Mardis, E.R., Sahinalp, S.C., and Unrau, P.J. (2008). Comparative analysis of the small RNA transcriptomes of *Pinus contorta* and *Oryza sativa*. Genome Res. **18:** 571–584.

Mosher, R.A., Schwach, F., Studholme, D., and Baulcombe, D.C. (2008). PolIVb influences RNA-directed DNA methylation independently of its role in siRNA biogenesis. Proc. Natl. Acad. Sci. USA **105:** 3145–3150.

Mukherjee, K., Campos, H., and Kolaczkowski, B. (2013). Evolution of animal and plant dicers: early parallel duplications and recurrent adaptation of antiviral RNA binding in plants. Mol. Biol. Evol. **30:** 627–641.

Nobuta, K., et al. (2008). Distinct size distribution of endogeneous siRNAs in maize: Evidence from deep sequencing in the *mop1-1* mutant. Proc. Natl. Acad. Sci. USA **105:** 14958–14963.

Nystedt, B., et al. (2013). The Norway spruce genome sequence and conifer genome evolution. Nature **497:** 579–584.

Pall, G.S., and Hamilton, A.J. (2008). Improved northern blot method for enhanced detection of small RNA. Nat. Protoc. **3**: 1077–1084.

Quinlan, A.R., and Hall, I.M. (2010). BEDTools: a flexible suite of utilities for comparing genomic features. Bioinformatics **26:** 841–842.

Rensing, S.A., et al. (2008). The Physcomitrella genome reveals evolutionary insights into the conquest of land by plants. Science **319**: 64–69.

Robinson, M.D., McCarthy, D.J., and Smyth, G.K. (2010). edgeR: a Bioconductor package for differential expression analysis of digital gene expression data. Bioinformatics **26:** 139–140.

Sambrook, J., and Russell, D.W. (2001). Molecular Cloning: A Laboratory Manual, 3rd ed. (Cold Spring Harbor, NY: Cold Spring Harbor Laboratory Press).

Talmor-Neiman, M., Stav, R., Klipcan, L., Buxdorf, K., Baulcombe, D.C., and Arazi, T. (2006). Identification of trans-acting siRNAs in moss and an RNA-dependent RNA polymerase required for their biogenesis. Plant J. **48:** 511–521.

Tamura, K., Peterson, D., Peterson, N., Stecher, G., Nei, M., and Kumar, S. (2011). MEGA5: molecular evolutionary genetics analysis using maximum likelihood, evolutionary distance, and maximum parsimony methods. Mol. Biol. Evol. **28:** 2731–2739.

Wierzbicki, A.T., Haag, J.R., and Pikaard, C.S. (2008). Noncoding transcription by RNA polymerase Pol IVb/Pol V mediates transcriptional silencing of overlapping and adjacent genes. Cell **135:** 635–648.

Wierzbicki, A.T., Ream, T.S., Haag, J.R., and Pikaard, C.S. (2009). RNA polymerase V transcription guides ARGONAUTE4 to chromatin. Nat. Genet. **41:** 630–634.

Xie, Z., Johansen, L.K., Gustafson, A.M., Kasschau, K.D., Lellis, A. D., Zilberman, D., Jacobsen, S.E., and Carrington, J.C. (2004). Genetic and functional diversification of small RNA pathways in plants. PLoS Biol. **2:** E104.

Zemach, A., McDaniel, I.E., Silva, P., and Zilberman, D. (2010). Genome-wide evolutionary analysis of eukaryotic DNA methylation. Science **328:** 916–919.

Zhang, H., et al. (2013). DTF1 is a core component of RNA-directed DNA methylation and may assist in the recruitment of Pol IV. Proc. Natl. Acad. Sci. USA **110:** 8290–8295.

Zhang, J., Zhang, S., Han, S., Li, X., Tong, Z., and Qi, L. (2013). Deciphering small noncoding RNAs during the transition from dormant embryo to germinated embryo in Larches (*Larix leptolepis*). PLoS One **8:** e81452.

Zong, J., Yao, X., Yin, J., Zhang, D., and Ma, H. (2009). Evolution of the RNA-dependent RNA polymerase (RdRP) genes: duplications and possible losses before and after the divergence of major eukaryotic groups. Gene **447:** 29–39.

A

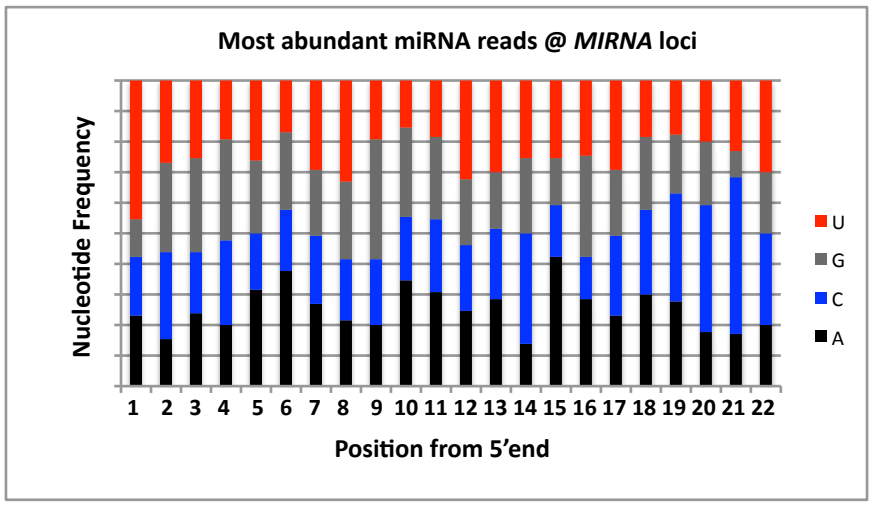

B

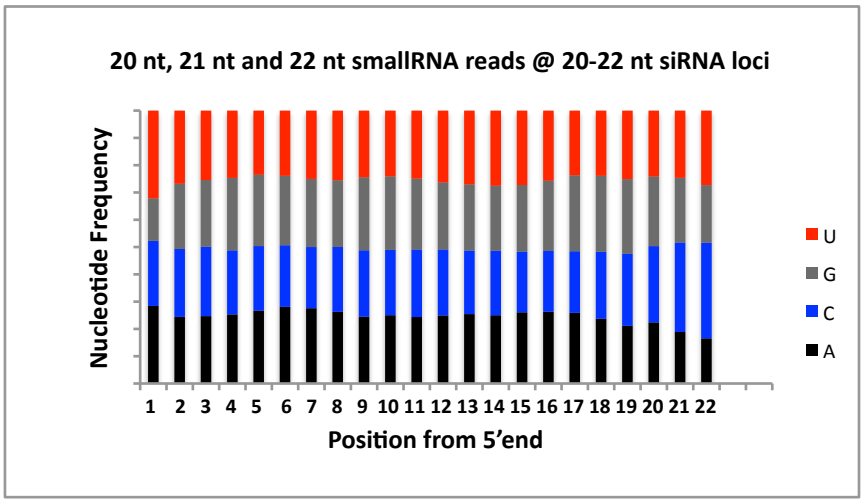

C

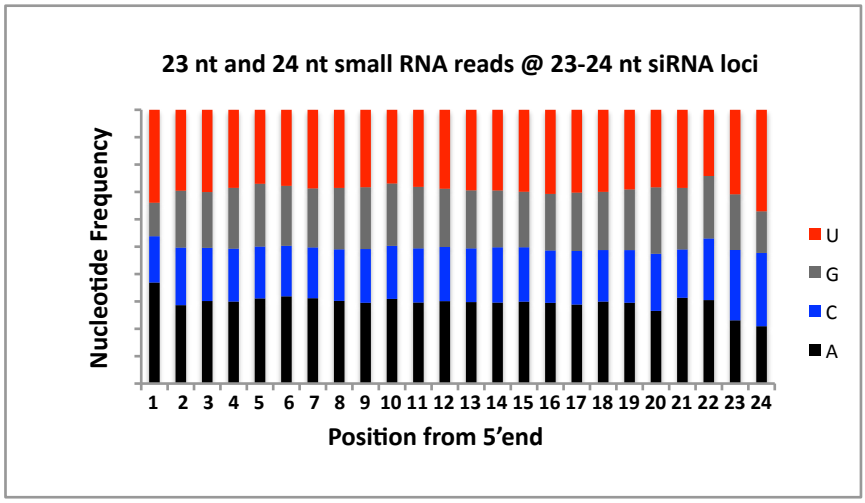

Supplemental Figure 1. Nucleotide frequency of *Physcomitrella patens* small RNAs for each position. Only distinct small RNA sequences were considered in this analysis.
Frequency of each nucleotide for each position in **(A)** most abundant miRNA reads at *MIRNA* loci **(B)** small RNA reads mapped to 20-22 nt siRNA loci and **(C)** 23-24 nt siRNA loci.

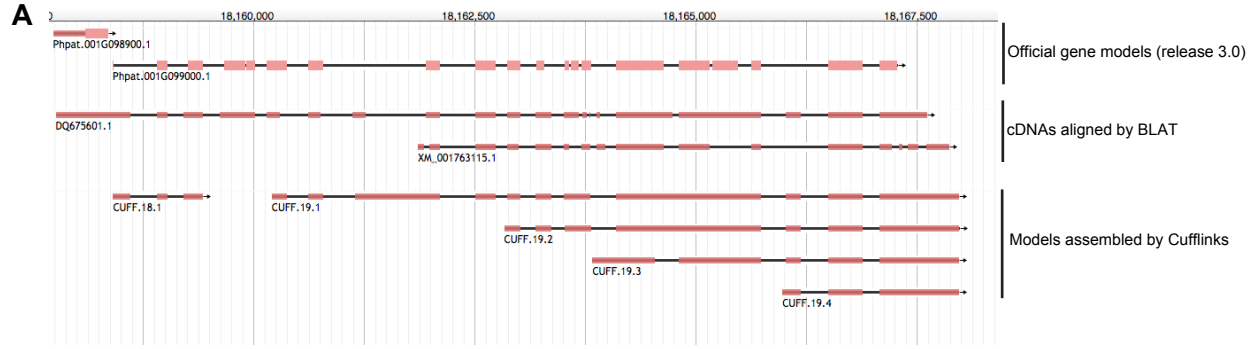
A
18,160,000
18,162,500
18,165,000
18,167,500
Phpat.001G098900.1
Phpat.001G099000.1
DQ675601.1
XM_001763115.1
CUFF.18.1
CUFF.19.1
CUFF.19.2
CUFF.19.3
CUFF.19.4
Official gene models (release 3.0)
cDNAs aligned by BLAT
Models assembled by Cufflinks

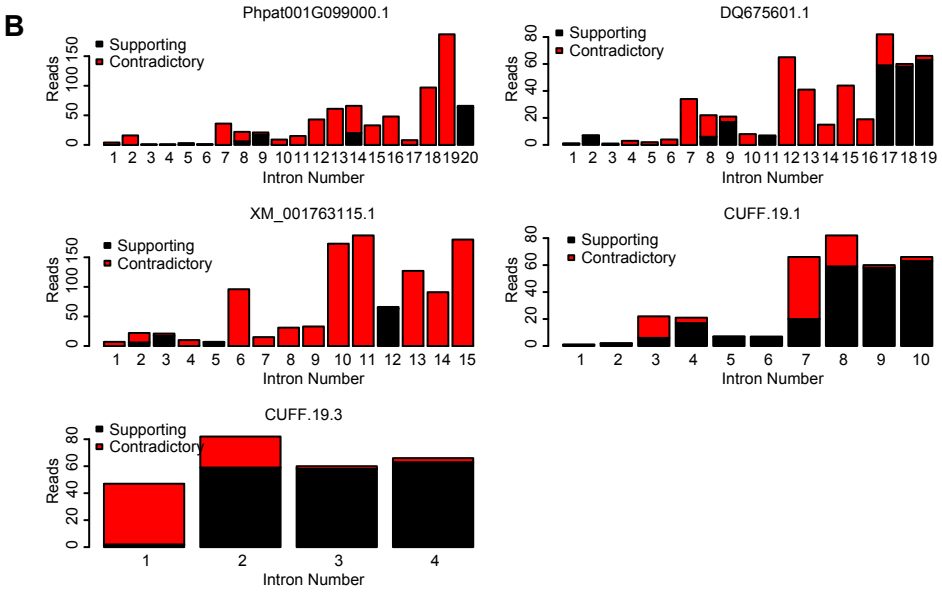
B
Phpat001G099000.1
DQ675601.1
XM_001763115.1
CUFF.19.1
CUFF.19.3
Supporting
Contradictory
Reads
Intron Number

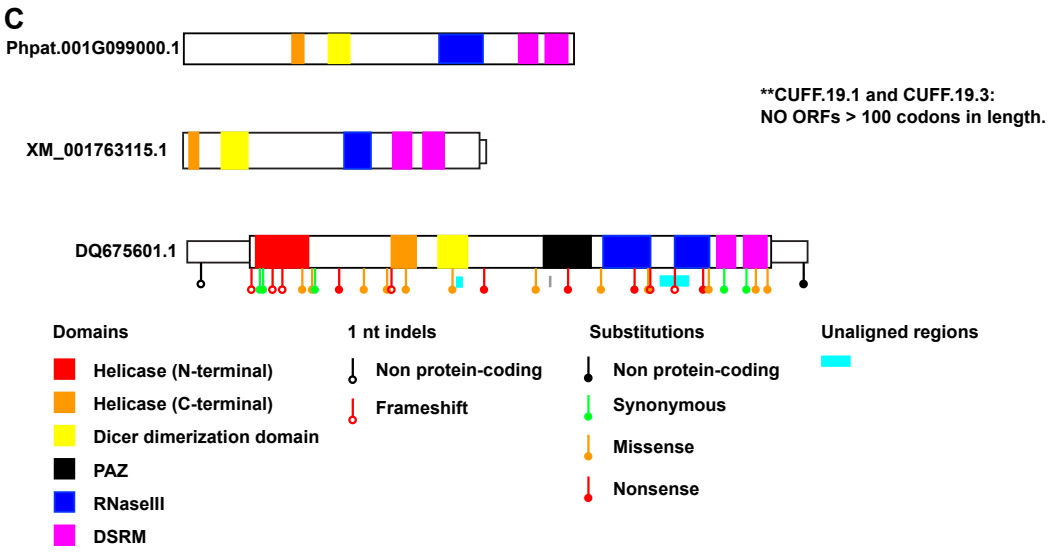
C
Phpat.001G099000.1
XM_001763115.1
DQ675601.1
**CUFF.19.1 and CUFF.19.3:
NO ORFs > 100 codons in length.
Domains
Helicase (N-terminal)
Helicase (C-terminal)
Dicer dimerization domain
PAZ
RNaseIII
DSRM
1 nt indels
Non protein-coding
Frameshift
Substitutions
Non protein-coding
Synonymous
Missense
Nonsense
Unaligned regions

Supplemental Figure 2. Discrepancies in Pp *DCL1b* annotations.
(A) Genome-browser snapshot of the *DCL1b* locus, showing various mRNA models. The region is roughly Chr01:18157500..18167930 **(B)** Barplots showing tallies of supporting and contradictory RNA-seq reads for each intron of the indicated gene models. RNA-seq data were from a merger of SRR435295 and SRR435296 (Chen et al., 2012), aligned to the reference genome using tophat (version 2.0.9) with non-default setting -I 5000 (using bowtie2 version 2.1.0 as the underlying alignment engine). Contradictory reads were those which had at least one base aligned to the intron, while confirmatory reads were those which spanned the annotated splice sites exactly. The RNA-seq alignments are downloadable from http://plantsmallrnagenes.psu.edu/Physcomitrella_patens/data/RNA-seq/Chen_et_al_WT.bam Note that the majority of introns for the first three models are unsupported by the empirical data. **(C)** Schematics, to scale, of inferred protein sequences from the indicated mRNA models. Protein domains were based on searches of the PFAM database (version 27; http://pfam.xfam.org/) under default parameters. mRNA model DQ675601.1 had multiple mismatches to the reference genome. The consequences of those edits are shown. Note that none of the gene models can make a full-length functional DCL protein. Phpat001G09900.1 and XM_001763115.1 lack the N-terminal Helicase domain, the PAZ domain, and one of the RNase III domains, while DQ675601.1 contains multiple frameshifts and premature stop codons.None of the the Cufflinks-assembled mRNAs have any ORFs longer than 100 codons.

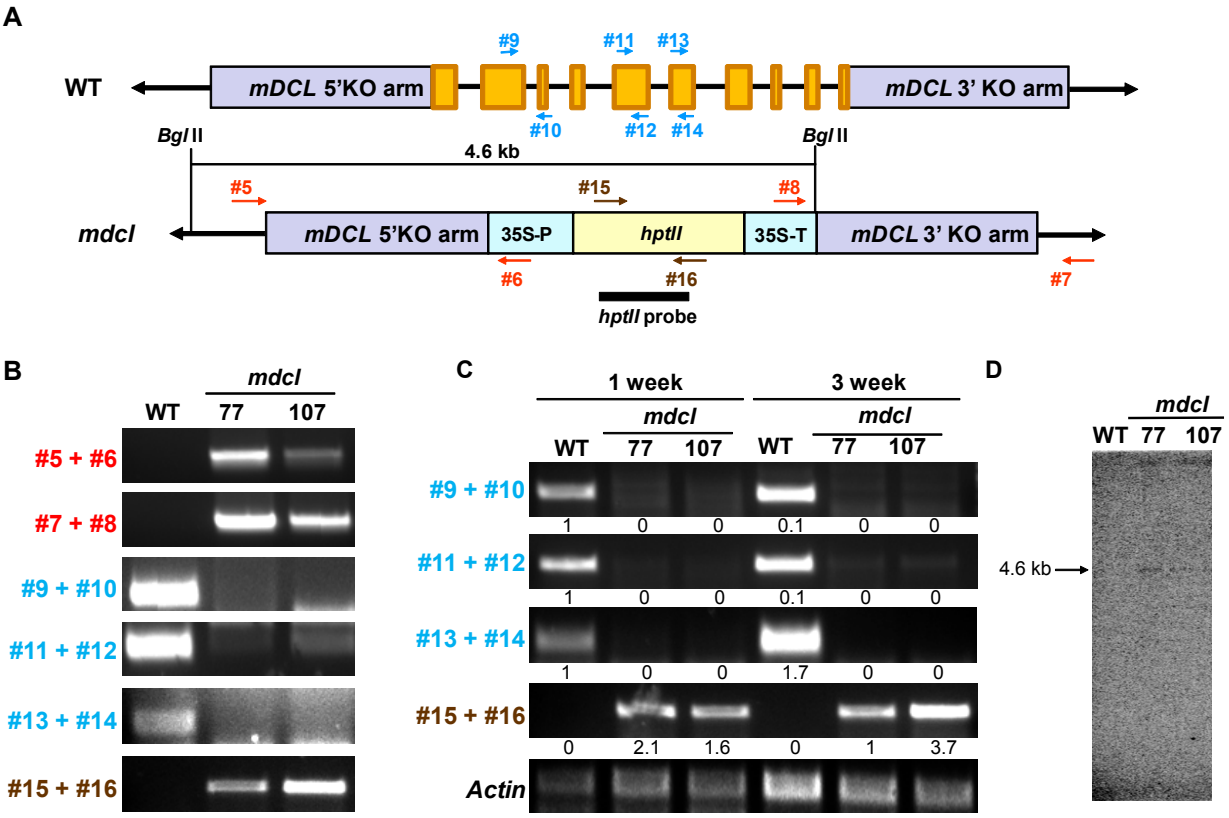

Supplemental Figure 3. Targeted knock-out of *mDCL*.
(A) Schematic of *mDCL* knock-out by homologous recombination. 77 and 107 correspond to different alleles of the *mdcl* mutant. The numbered arrows indicate approximate locations of primers (Supplemental Table 3). 35S-P, CaMV 35S promoter; 35S-T, CaMV 35S terminator. **(B)** Genotyping of transformed plants by genomic DNA PCRs using the indicated primer sets. **(C)** Transcript analysis by RT-PCR using indicated primer sets. *Actin* served as a control. Numbers below PCR fragments indicate relative (to *Actin*) intensities of bands compared to 1-week old WT, except for primer set 15-16, which was normalized to the value of 3-week *mdcl* line 77. **(D)** DNA blot analysis of *mdcl* mutant plants. BglII digested genomic DNA was blotted and hybridized with an *hptII* probe.

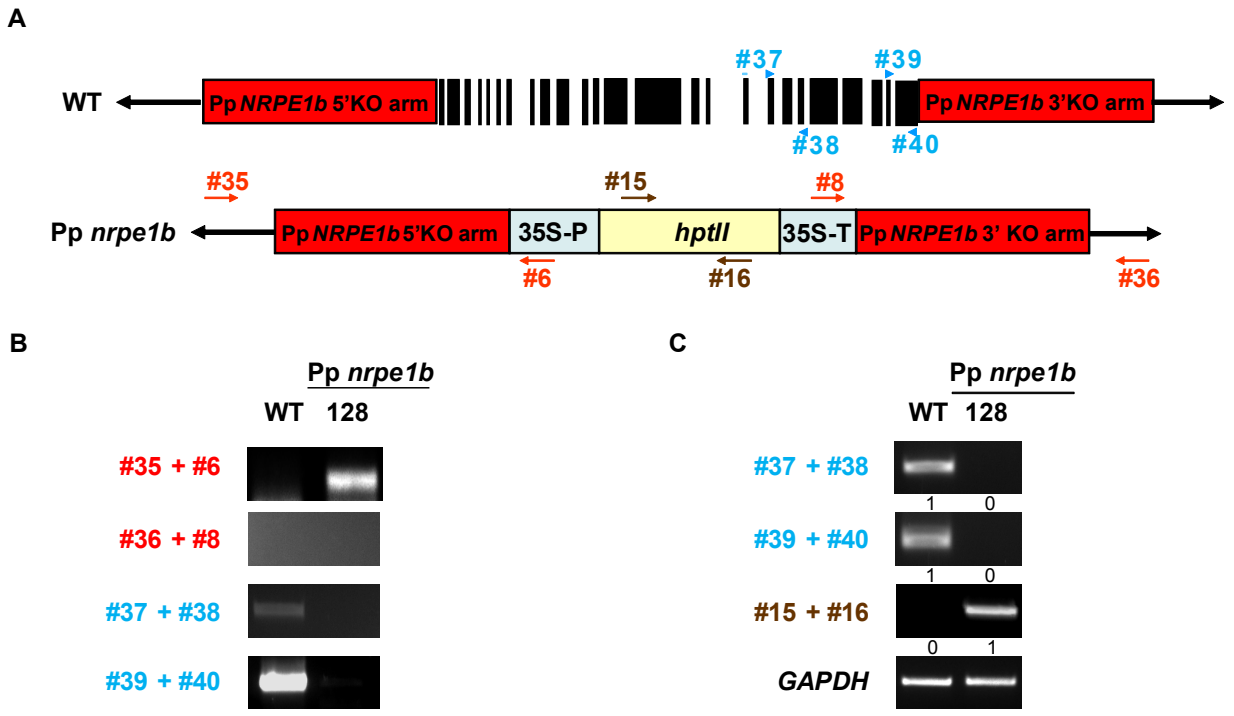

Supplemental Figure 4. Targeted knock-out of Pp *NRPE1b*
(A) Schematic of Pp *NRPE1b* knock out by homologous recombination. The numbered arrows indicate approximate locations of primers (Supplemental Table 3). 35S-P, CaMV 35S promoter; 35S-T, CaMV 35S terminator. **(B)** Genotyping of transformed plants by genomic DNA PCRs using the indicated primer sets. '128' referes to the isolated mutant line. **(C)** Transcript analysis by RT-PCR using indicated primer sets. *GAPDH* served as a control. Numbers below PCR fragments indicate relative intensity (normalized to *GAPDH*) compared to that of WT (primer sets 37-38 and 39-40) or mutant (primer set 15-16).

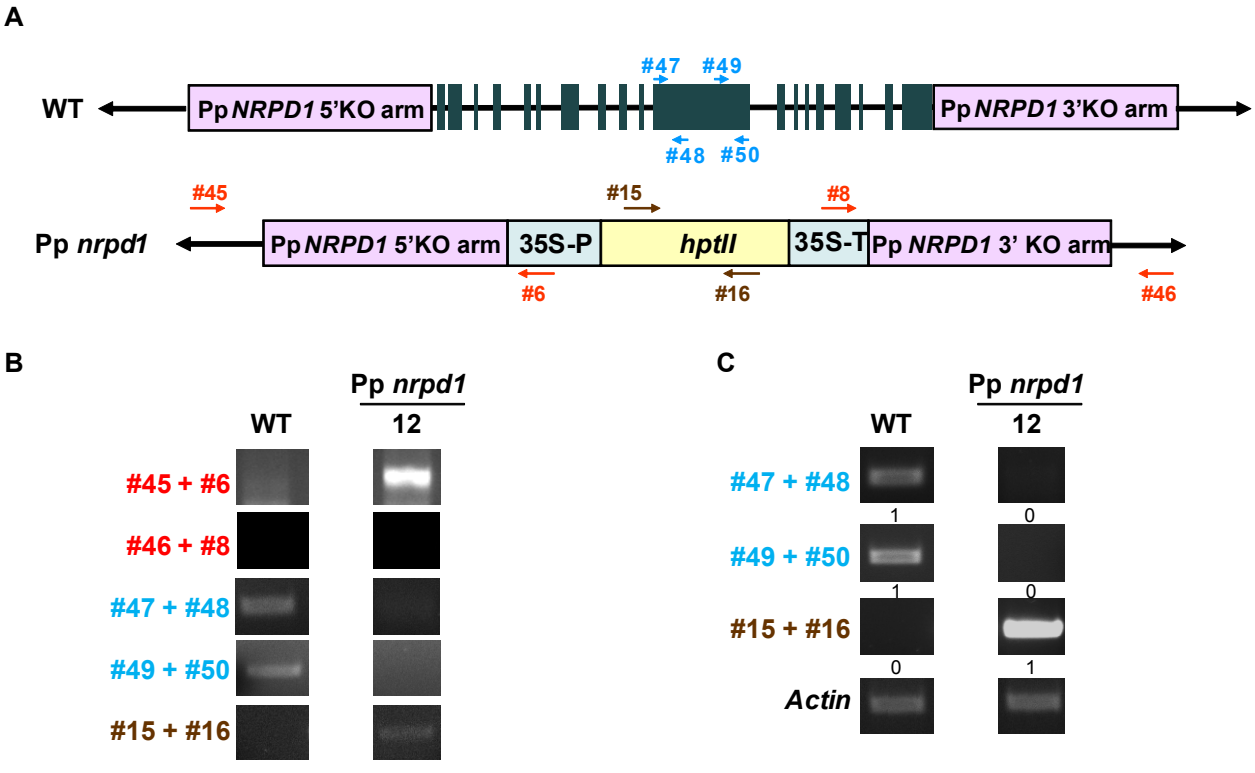

Supplemental Figure 5. Targeted knock-out of Pp *NRPD1*.
(A) Schematic of Pp *NRPD1* knock out by homologous recombination. The numbered arrows indicate approximate locations of primers (Supplemental Table 3). 35S-P, CaMV 35S promoter; 35S-T, CaMV 35S terminator. **(B)** Genotyping of transformed plants by genomic DNA PCRs using the indicated primer sets. Both 5' and 3' recombination in line 12 was confirmed. **(C)** Transcript analysis by RT-PCR using indicated primer sets. *Actin* served as a control. Numbers below PCR fragments indicate relative intensity (normalized to *Actin*) compared to that of WT (primer sets 47-48 and 49-50) or mutant (primer set 15-16).

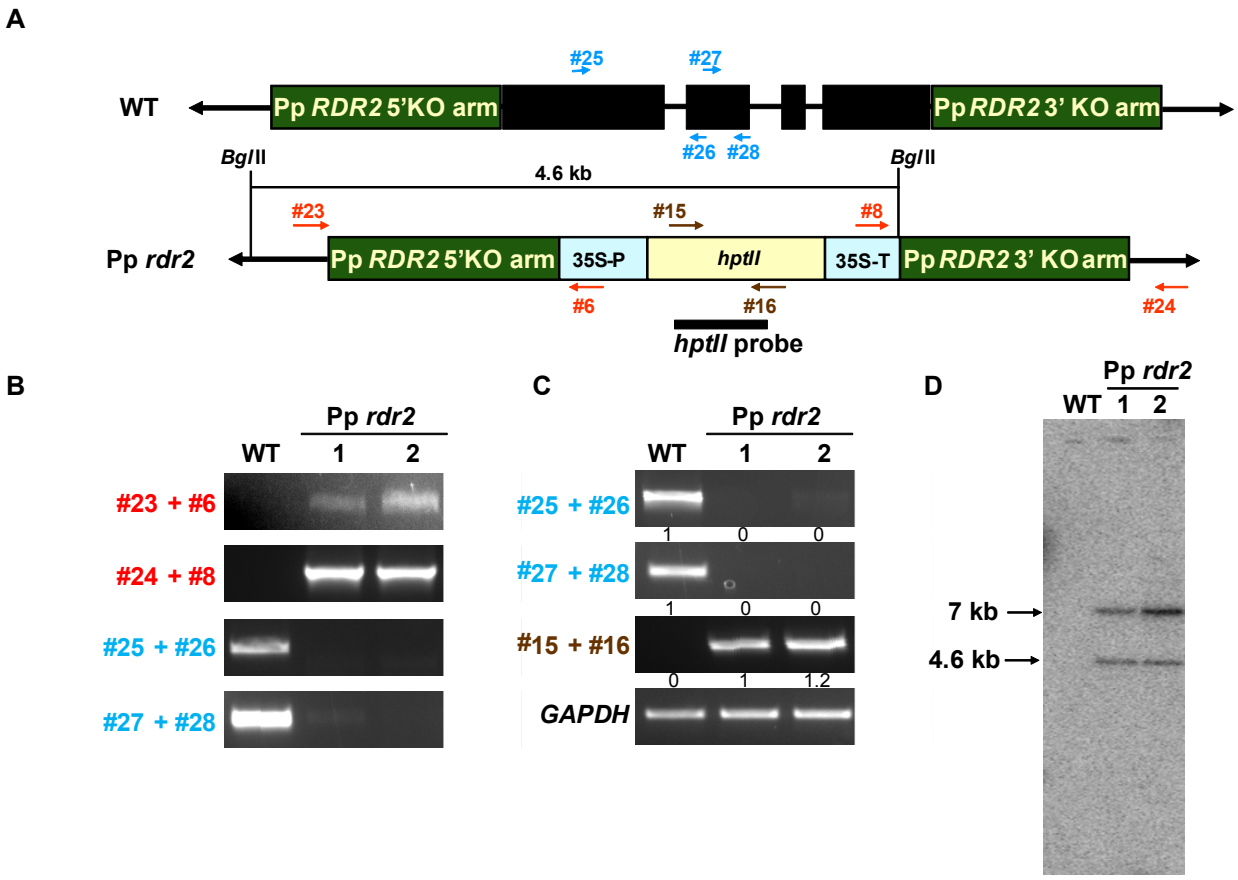

Supplemental Figure 6. Targeted knock-out of Pp *RDR2*.
(A) Schematic of Pp *RDR2* knock out by homologous recombination. The numbered arrows indicate approximate locations of primers (Supplemental Table 3). 35S-P, CaMV 35S promoter; 35S-T, CaMV 35S terminator. **(B)** Genotyping of transformed plants by genomic DNA PCRs using the indicated primer sets. '1' and '2' refer to two independent lines **(C)** Transcript analysis by RT-PCR using indicated primer sets. *GAPDH* served as a control. Numbers below PCR fragments indicate relative intensity (compared to *GAPDH*) compared to that of WT (primer sets 25-26 and 27-28) or mutant line 1 (primer set 15-16). **(D)** DNA blot analysis. BglII digested genomic DNA was blotted and hybridized with an *hptII* probe. The 7kb band corresponds to the fragment size for the tandem repeat of the targeting cassette. This result shows the vector was inserted into a single site with a tandem repeat in the genome.

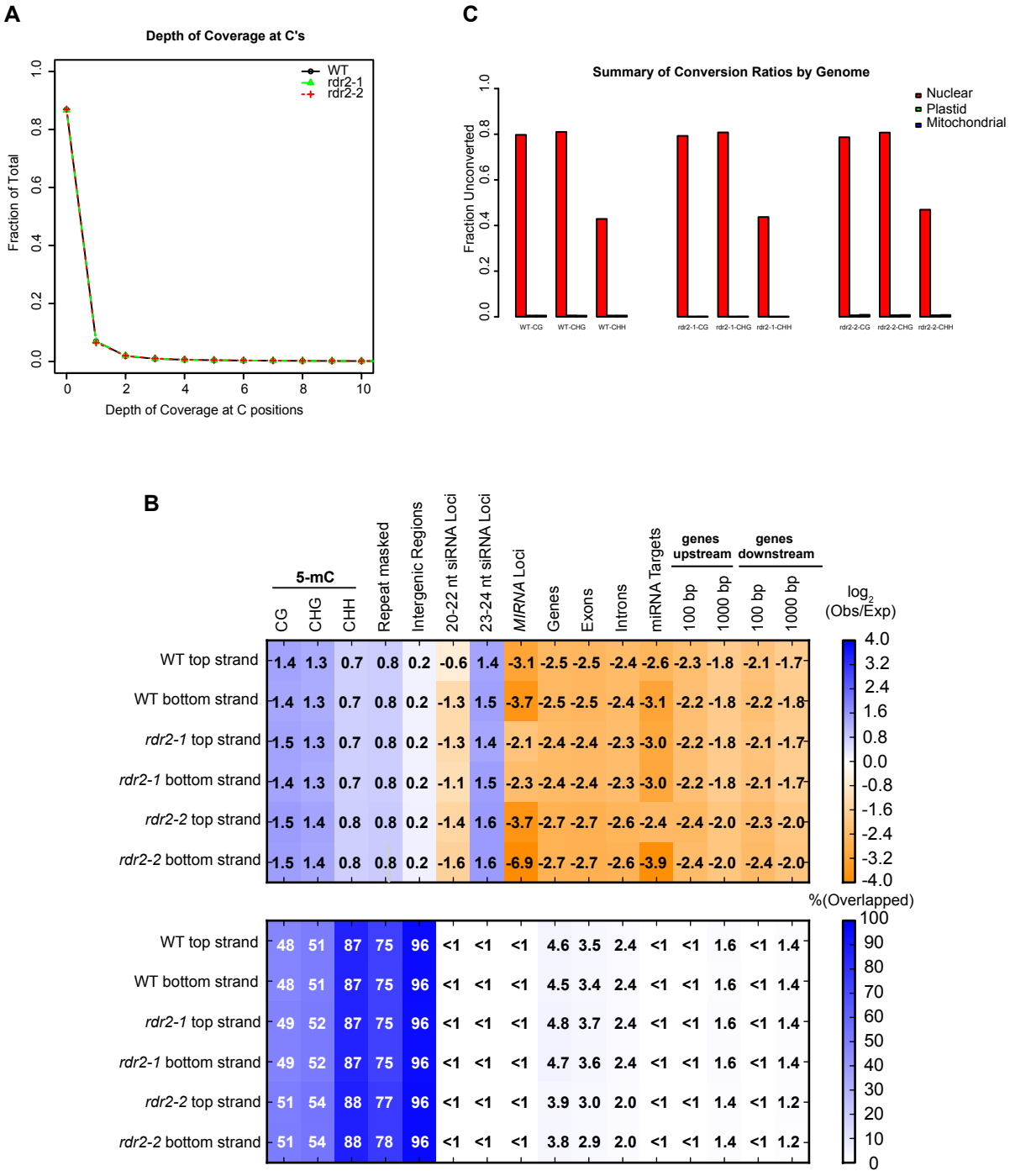

Supplemental Figure 7. Overview of bisulfite-seq libraries. **(A)** Overall depth of coverage at cytosines in the nuclear genome. **(B)** Heatmap showing log2 (observed overlapped bases / expected overlapped bases) for each of the pair-wise comparisons shown (top), and percentages of covered regions that overlap indicated regions (bottom). **(C)** Summary of conversion ratios by genome and library.

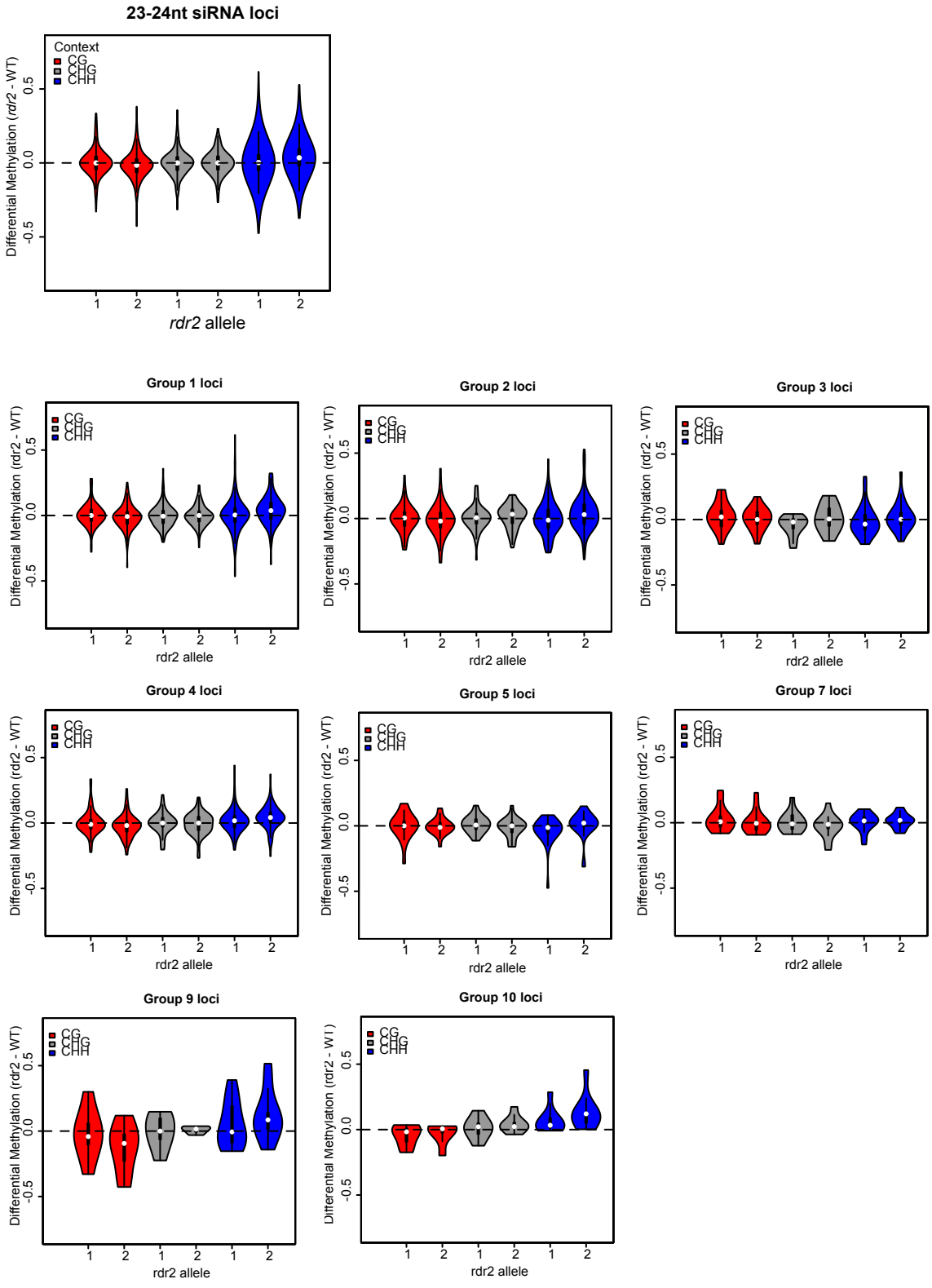

Supplemental Figure 8. Analysis of DNA methylation at 23-24 nt siRNA loci in Pp *rdr2* mutants. Differential DNA methylation between the indicated Pp *rdr2* alleles and the wild-type for the indicated loci. The 'groups' refer to groups shown in Figure 6D. Violin plots show a Tukey boxplot (line=median, box edges=1st and 3rd quartiles, whiskers=1.5 IQR) surrounded by a twinned kernel density plot to visually show the distribution of the data.

Supplemental Data. Coruh et al. Plant Cell (2015) 10.1105/tpc.15.00228

Supplemental Table 1: *Physcomitrella patens* small RNA-seq libraries.

Library	Genotype	Strain	Number of Mapped Reads	GEO GSE	GEO GSM	Libraries Re-sequenced
1	Wild-type	Gransden 2004	29,985,916	GSE44900	GSM1093595	-
2	Wild-type	Gransden 2004		GSE44900	GSM1194292	Re-run of Library 1
3	Wild-type	Gransden 2004	31,363,125	GSE44900	GSM1093596	-
4	Wild-type	Gransden 2004		GSE44900	GSM1194293	Re-run of Library 3
5	Wild-type	Gransden 2004	10,487,292	GSE44900	GSM1194296	-
6	Wild-type	Gransden 2004	12,655,162	GSE44900	GSM1194297	-
7	Wild-type	Gransden 2009	19,593,167	GSE44900	GSM1093597	-
8	Wild-type	Gransden 2009		GSE44900	GSM1194294	Re-run of Library 7
9	Wild-type	Gransden 2009	24,811,895	GSE44900	GSM1093598	-
10	Wild-type	Gransden 2009		GSE44900	GSM1194295	Re-run of Library 9
11	rdr2-1	Gransden 2004	22,023,647	GSE51419	GSM1245155	-
12	rdr2-1	Gransden 2004		GSE51419	GSM1245157	Re-run of Library 11
13	rdr2-1	Gransden 2004	29,305,900	GSE51419	GSM1245156	-
14	rdr2-1	Gransden 2004		GSE51419	GSM1245158	Re-run of Library 13
15	rdr2-2	Gransden 2004	16,328,990	GSE51419	GSM1245159	-
16	rdr2-2	Gransden 2004	17,532,117	GSE51419	GSM1245160	-
17	rdr6-19	Gransden 2004	12,771,158	GSE51419	GSM1245161	-
18	rdr6-19	Gransden 2004	10,799,819	GSE51419	GSM1245162	-
19	rdr6-35	Gransden 2004	12,976,974	GSE51419	GSM1245163	-
20	rdr6-35	Gransden 2004	14,889,594	GSE51419	GSM1245164	-
21	dcl3-5	Gransden 2004	11,234,135	GSE51419	GSM1245131	-
22	dcl3-5	Gransden 2004	12,369,785	GSE51419	GSM1245132	-
23	dcl3-10	Gransden 2004	22,572,662	GSE51419	GSM1245133	-
24	dcl3-10	Gransden 2004	12,409,186	GSE51419	GSM1245134	-
25	dcl4-1	Gransden 2004	8,549,049	GSE51419	GSM1245135	-
26	dcl4-1	Gransden 2004	15,871,722	GSE51419	GSM1245136	-
27	mdcl-77	Gransden 2009	25,765,988	GSE51419	GSM1245137	-
28	mdcl-77	Gransden 2009		GSE51419	GSM1245141	Re-run of Library 27
29	mdcl-77	Gransden 2009	24,688,556	GSE51419	GSM1245138	-
30	mdcl-77	Gransden 2009		GSE51419	GSM1245142	Re-run of Library 29
31	mdcl-107	Gransden 2009	39,984,388	GSE51419	GSM1245139	-
32	mdcl-107	Gransden 2009		GSE51419	GSM1245143	Re-run of Library 31
33	mdcl-107	Gransden 2009	25,387,913	GSE51419	GSM1245140	-
34	mdcl-107	Gransden 2009		GSE51419	GSM1245144	Re-run of Library 33
35	nrpe1b_128	Gransden 2004	29,803,961	GSE51419	GSM1245145	-
36	nrpe1b_128	Gransden 2004		GSE51419	GSM1245149	Re-run of Library 35
37	nrpe1b_128	Gransden 2004	26,708,434	GSE51419	GSM1245146	-
38	nrpe1b_128	Gransden 2004		GSE51419	GSM1245150	Re-run of Library 37
39	nrpd1_12	Gransden 2004	13,482,499	GSE51419	GSM1245153	-
40	nrpd1_12	Gransden 2004	15,407,223	GSE51419	GSM1245154	-

Supplemental Data. Coruh et al. Plant Cell (2015) 10.1105/tpc.15.00228
Supplemental Table 2: Summary of whole-genome bisulfite-seq libraries

Sample	SRA Accession	Total Pairs	Pairs Passed Quality Control	Concordantly Aligned Pairs	Pairs flagged as PCR Duplicates	Accepted Pairs
Wild-type	*SRR2013850*	222,081,099	211,783,332	156,513,930	153,613,143	2,900,787
rdr2-1	*SRR2013877*	235,045,740	224,132,719	202,792,076	199,510,574	3,281,502
rdr2-2	*SRR2013879*	259,564,115	245,949,602	199,155,549	195,904,139	3,251,410

Supplemental Data. Coruh et al. Plant Cell (2015) 10.1105/tpc.15.00228

Supplemental Table 3. Oligonucleotide sequences used in this study.

Number	Use	Sequence (5'→3')
1	mDCL KO vector construction, 5'KO arm (Forward)	CGCCTAGGATTTAAATAGATGTGTATTAATTACACCAACAC
2	mDCL KO vector construction, 5'KO arm (Reverse)	CGAAGCTTAATGATGATACAGGGGTGACAACGG
3	mDCL KO vector construction, 3'KO arm (Forward)	CGAGATCTCTTTATAGAAGGCATCTAGGAAGTC
4	mDCL KO vector construction, 3'KO arm (Reverse)	CGACGCGTATTTAAATTACAATAGATTAATTTTCATACAAA
5	mDCL KO identification of checking for 5' recombination (Forward)	ACCTCCAACGAGATGAGAACTACGC
6	KO identification checking for 5' recombination, 35S Promoter Internal (Revei	AGATAGCTGGGCAATGGAATCCGA
7	mDCL KO identification of checking for 3' recombination (Reverse)	AATATCCGCGCAGGTTAAGTTCCTAGC
8	KO identification checking for 3' recombination, 35S Terminator Internal (Forv	GGGTTTCGCTCATGTGTTGAGCAT
9	mDCL KO genotyping (Internal Forward1)	GAAGCACTCGATGGTGGTGG
10	mDCL KO genotyping (Internal Reverse1)	ACTGCAGATGTTCGCCGTACGTAG
11	mDCL KO genotyping (Internal Forward2)	GGGCAAGTCATTGGACTCAAAACC
12	mDCL KO genotyping (Internal Reverse2)	CTTCCTCTTGGTACACCGCTC
13	mDCL KO genotyping (Internal Forward3)	GCATGTGAAGGGAACCACTCATAC
14	mDCL KO genotyping (Internal Reverse3)	CGTCTTGGTATTTAGCAGTTCAGC
15	Identification of hptII gene in mutants (Forward)	TGTTTATCGGCACTTTGCATCGGC
16	Identification of hptII gene in mutants (Reverse)	AGCTGCATCATCGAAATTGCCGTC
17	Actin (Forward)	ATCTGGAATGGTCAAGGCCGGTTT
18	Actin (Reverse)	TCATCTTCTCCCTGTTCGCCTTCG
19	RDR2 KO vector construction, 5'KO arm (Forward)	CAAGCTTGGGACAAGGGAAGAGGTTCTCAAA
20	RDR2 KO vector construction, 5'KO arm (Reverse)	AACTCGAGACACCCACCACATTCCTCAGTCAT
21	RDR2 KO vector construction, 3'KO arm (Forward)	CCAGATCTACTGCTACACAGCGAGGATTTCTG
22	RDR2 KO vector construction, 3'KO arm (Reverse)	CCACGCGTTCAAGCAATGGGATAGGAGGCCAA
23	RDR2 KO identification of checking for 5' recombination (Forward)	GAGAGATGCAGTTTCGCAGCAGTA
24	RDR2 KO identification of checking for 3' recombination (Reverse)	TGGCTATATGTATGGTAATAAGGGACC
25	RDR2 KO genotyping (Internal Forward1)	ACAATGATCAGGGCATGGATGGGA
26	RDR2 KO genotyping (Internal Reverse1)	ACCCGCTGCGAGCATATCTATCAA
27	RDR2 KO genotyping (Internal Forward2)	TGATAGATATGCTCGCAGCGGGTT
28	RDR2 KO genotyping (Internal Reverse2)	AAACCAAGCAGTCAACCATGTGCC
29	GAPDH F	CCTCTTGCAAAGGTGATCAACGAC
30	GAPDH R	ACCACACGGTTGCTGTAACCCCAC
31	NRPE1a KO vector construction, 5'KO arm (Forward)	GGAAGCTTCCGGAAGAATTTGGCTAATCCGCA
32	NRPE1a KO vector construction, 5'KO arm (Reverse)	GGCTCGAGCGAGCGATAAGCATTAAAGCAACG
33	NRPE1a KO vector construction, 3'KO arm (Forward)	GGAGATCTTGCGTGAAACCTATTTGAGATGGA
34	NRPE1a KO vector construction, 3'KO arm (Reverse)	GGACGCGTGCCACAAGTCCAAGACATTAGAACT
35	NRPE1a KO identification of checking for 5' recombination (Forward)	TCTGTTGTTGCTGATGCAGGTCAG
36	NRPE1a KO identification of checking for 3' recombination (Reverse)	GTGTCTTCAAGCTAGACATATTTAGAAATGG
37	NRPE1a KO genotyping (Internal Forward1)	GGGACAAATTTTCTTTTGTGTCAGTTA
38	NRPE1a KO genotyping (Internal Reverse1)	AATACCAAACCAAGTCTCTGTGAG
39	NRPE1a KO genotyping (Internal Forward2)	AACTTGGTGGCAGGCTTTCTGACG
40	NRPE1a KO genotyping (Internal Reverse2)	TCAAGATCCTCATGATCAATAGGC
41	NRPD1 KO vector construction, 5'KO arm (Forward)	GGCCTAGGTGTCATTTAGGATAGTGCGGG
42	NRPD1 KO vector construction, 5'KO arm (Reverse)	GGCTCGAGCCTTCAAGCACAAAAACAAAG

43	NRPD1 KO vector construction, 3'KO arm (Forward)	GGAGATCTGATTGGTTACCTTCGCAATGCCAT		
44	NRPD1 KO vector construction, 3'KO arm (Reverse)	GGACGCGTGCAATTTGATGGCTCCTTGT		
45	NRPD1 KO identification of checking for 5' recombination (Forward)	TGTGAAGGCAGTTAATGGTGA		
46	NRPD1 KO identification of checking for 3' recombination (Reverse)	GGAGATGGATACTATGATTGATGG		
47	NRPD1 KO genotyping (Internal Forward1)	AGATACATGAAGGGGCATATTTTAGC		
48	NRPD1 KO genotyping (Internal Reverse1)	GTCGTTCAATATTAAAAGCCGTGAC		
49	NRPD1 KO genotyping (Internal Forward2)	TTGGATAAGGTTGCTGTCGATAGG		
50	NRPD1 KO genotyping (Internal Reverse2)	ACCATACCGTGATGATAAAGTGTG		
51	Small RNA gel blot of ppt-miR156 (probe)	GTGCTCACTCTCTTCTGTCA		
52	Small RNA gel blot U6 (probe)	TTGTGCGTGTCATCCTTGCGCA		
53	Small RNA gel blot SBP3 up target region F (probe)	GTATCCCTGCCCTTCAACTTCAGGTTGGTTTTATGTTTGTCGAAACAGCT		
54	Small RNA gel blot SBP3 up target region R (probe)	AGCTGTTTCGACAAACATAAAACCAACCTGAAGTTGAAGGGCAGGGATAC		
55	Small RNA gel blot SBP3 down target region F (probe)	TGAGTCTGTGGGGCTGAATTGTGGGCTAGCTGCGACTGGTTACGGGGCTC		
56	Small RNA gel blot SBP3 down target region R (probe)	GAGCCCCGTAACCAGTCGCAGCTAGCCCACAATTCAGCCCCACAGACTCA		
57	Small RNA gel blot HD-ZIPIII up target site F (probe)	CAACGCAAGGAAGCAACAAGGCTGGTCAGTGTTAATGCAAAGCTGACAGC		
58	Small RNA gel blot HD-ZIPIII up target site R (probe)	GCTGTCAGCTTTGCATTAACACTGACCAGCCTTGTTGCTTCCTTGCGTTG		
59	Small RNA gel blot HD-ZIPIII down target site F (probe)	GATTACTGTACTTTGAGATACACTACAATTTTGGAGGATGGAAACCTGGT		
60	Small RNA gel blot HD-ZIPIII down target site R (probe)	ACCAGGTTTCCATCCTCCAAAATTGTAGTGTATCTCAAAGTACAGTAATC		
61	Sequencing primer A*	ACACTCTTTCCCTACACGACGCTCTTCCGATCT		
62	Sequencing primer B*	CGGTCTCGGCATTCCTGCTGAACCGCTCTTCCGATCT		
63	Illumina PE PCR primer A	AATGATACGGCGACCACCGAGATCTACACTCTTTCCCTACACGACGCTCTTCCGATCT		
64	Illumina PE PCR primer B	CAAGCAGAAGACGGCATACGAGATCGGTCTCGGCATTCCTGCTGAACCGCTCTTCCGATCT		
65	RT3 Forward	AACCATGGTCTTCTRTTTCTATGGAYTTCATCA		
66	RT3 Reverse	CCAAAATCTTGATACAAATTGAGT		
67	RT6 Forward	TATGATTGCGCCATAGAMTTRSARGAAGGA		
68	RT6 Reverse	AAAATATCATCYARRTAGATGACAACAAA		
69	Pp EF1-alpha Forward	CGACGCCCCTGGACATC		
70	Pp EF1-alpha Reverse	CCTGCGAGGTTCCCGTAA		
*	C's were synthesized as 5-methyl Cytosine			

Comprehensive Annotation of *Physcomitrella patens* Small RNA Loci Reveals That the Heterochromatic Short Interfering RNA Pathway Is Largely Conserved in Land Plants

Ceyda Coruh, Sung Hyun Cho, Saima Shahid, Qikun Liu, Andrzej Wierzbicki and Michael J. Axtell

Plant Cell; originally published online July 24, 2015;
DOI 10.1105/tpc.15.00228